Late Middle Miocene volcanism in Northwest Borneo, Southeast Asia: Implications for tectonics, paleoclimate and stratigraphic marker

Mu. Ramkumar, M. Santosh, R. Nagarajan, S. Li, M. Mathew, D. Menier, N. Siddiqui, J. Rai, A. Sharma, S. Farroqui, et al.

HAL Id: hal-01919549
https://hal.univ-brest.fr/hal-01919549

Submitted on 12 Apr 2021

Accepted Manuscript

Late Middle Miocene volcanism in Northwest Borneo, Southeast Asia: Implications for tectonics, paleoclimate and stratigraphic marker

Mu. Ramkumar, M. Santosh, R. Nagarajan, S.S. Li, M. Mathew, D. Menier, N. Siddiqui, J. Rai, A. Sharma, S. Farroqui, M.C. Poppelreiter, J. Lai, V. Prasad
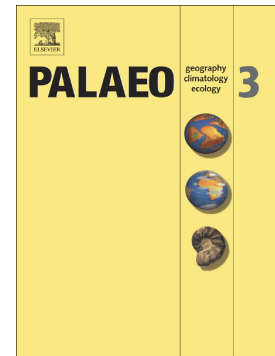
Please cite this article as: Mu. Ramkumar, M. Santosh, R. Nagarajan, S.S. Li, M. Mathew, D. Menier, N. Siddiqui, J. Rai, A. Sharma, S. Farroqui, M.C. Poppelreiter, J. Lai, V. Prasad , Late Middle Miocene volcanism in Northwest Borneo, Southeast Asia: Implications for tectonics, paleoclimate and stratigraphic marker. The address for the corresponding author was captured as affiliation for all authors. Please check if appropriate. Palaeo(2017), doi:10.1016/j.palaeo.2017.10.022

Late Middle Miocene volcanism in Northwest Borneo, Southeast Asia: Implications for tectonics, paleoclimate and stratigraphic marker

Mu.Ramkumar*[1,2], M.Santosh[3,4], R. Nagarajan[5], S.S. Li[3], M. Mathew[6], D. Menier[6], N.Siddiqui [7], J. Rai[8], A. Sharma[8], S.Farroqui[8], M.C.Poppelreiter[2], J.Lai[2], V.Prasad[8]

[1]Department of Geology, Periyar University, Salem – 636011. India. muramkumar@yahoo.co.in

[2]South East Asia Carbonate Research Laboratory (SEACaRL), Universiti Teknologi Petronas, Tronoh, Malaysia. M.Poppelreiter@SHELL.com; jonathanlai.c.m@gmail.com

[3]China University of Geosciences, Beijing, PR China. santosh@cugb.edu.cn; lishanshan199811@163.com

[4]Department of Earth Sciences, University of Adelaide, Adelaide SA 5005, Australia

[5]Department of Applied Geology, Curtin University, Sarawak, Malaysia. nagarajan@curtin.edu.my

[6]Laboratoire Géosciences Océan, UMR CNRS 6538, Université de Bretagne Sud, 56017 Vannes Cedex, France. dmenier5@gmail.com; manoj_mathew7@yahoo.com

[7]Department of Geoscience, Universiti Teknologi Petronas, Tronoh, Malaysia.numairpng@gmail.com

[8]Birbal Sahni Institute of Palaeosciences, 53 University Road, Lucknow. India. Jyotsana_rai@yahoo.com; anupam110367@gmail.com; shazi3112@gmail.com; prasad.van@gmail.com

* Corresponding Author.

Abstract

Explosive volcanic events often produce pyroclastic materials that can be recognized from the geological record. These discrete pyroclastics form regional marker beds. Here we report the occurrence of a tephra layer interbedded within very thick coal beds near Mukah, Sarawak, Borneo. Traceable for tens of kilometers in the Mukah area of Sarawak, this tephra layer can be considered as regional stratigraphic marker with precise chronostratigraphic control. Systematic sedimentological, mineralogical, geochemical and zircon U-Pb geochronological studies have revealed a major effusive volcanic event during the latest Middle Miocene, presumably contemporaneous and/or related to a magmatic event of an earlier phase of the Mt. Kinabalu pluton or magmatism in West Sarawak or East Sabah. The volcanic event had promoted catastrophic flooding of coastal swamps and fall-out from the ash clouds that formed a regionally monotonous tephra layer across the Serravallian- Tortonian boundary. In conjunction with the regional occurrences of trap rocks, structural trends and known tectonic events, we constrained the regional depositional environments, and climate. The tephra layer was deposited in a coastal plain-swamp,-seasonal, shallow, high-moderate energy fluvial channel-lacustrine environmental setting, wherein atmospheric fallout and eroded material from regoliths formed over older basement and volcanic rocks of the hinterland which were mixed to produce the tephra layer. This tephra layer is sandwiched between the very thick coal beds. A pre-existent volcanic chamber that was active for a long time, also experienced periodic explosive activity from probably the same magma chamber and conduit and including a major explosive activity that recycled early-formed crystals and felsic magma (rhyolite-dacite) during the major effusive event are also recognized. Our findings provide robust evidence for the prevalence of intensive chemical weathering under a wet-humid climate, and relative tectonic quiescence before the major effusive event, and the existence of vast, monotonously gently-sloping coastal plains and luxuriant vegetation akin to the present.

Key Words: Volcanic tephra dispersal, Zircon geochronology, Middle Miocene tectonics, coastal swamp, paleoclimate, NW Borneo.

1. Introduction

The Middle-Late Miocene was a period of atmospheric CO_2 draw down from ~650 ppm to ~100 ppm (Royer, 2006), perhaps due to the development of extensive swamp-peat deposition that promoted the transfer of carbon from the atmosphere and biosphere to the lithosphere as well as through intensive weathering that promoted lithogenic consumption of atmospheric CO_2. This period was also the time of rapid uplift of most mountain ranges in and around SE Asia (Kessler and Jong, 2015; Wang et al., 2017) that changed the climate of the region while other parts of the world continued to cool (Hay et al., 2002; Liu et al., 2017). Rapid and intense environmental perturbations such as large volcanic events affected the biotic and environmental conditions (Shen et al., 2012), and at times led to ecosystem collapse (Perrier et al., 2012). The Middle-Late Miocene period has also experienced perturbations in terms of extensive volcanism that transferred enormous quantities of gases into the atmosphere. Tephra layers originating from these massive effusive events are often preserved in stratigraphic records and help reconstruct past volcanism, including eruption frequency and magnitude, volume of erupted pyroclastic material, and the geochemical evolution of volcanoes (Kilian et al., 2003; Stern, 2008; Molloy et al., 2009; Watt et al., 2013; Bertrand et al., 2014; Weller et al., 2014).

In this study, we report a major volcanic event that lasted for ~320 kyr as evidenced by the occurrence of a regionally extensive 6-cm-thick volcanic tephra deposit preserved within ancient swamp and lacustrine settings in NW Borneo (Fig. 1). Based on multidisciplinary studies we have constrained the provenance, tectonic setting, depositional and paleoclimatic conditions.

Fig. 1.

2. Regional setting

The tectonically complex Borneo Island is the third largest island in the World, shared by Malaysia (the states of Sarawak and Sabah), Indonesia (Kalimantan) and Brunei (Fig. 1). Vastly inaccessible tropical rainforests, mountains and deep valleys inhibit geological research in this region (Mathew et al., 2016a). Plate boundaries, marginal ocean basins and arc systems (Fuller et al., 1999; Nagarajan et al., 2014) surround this region. This region has experienced significant tectonic activity (Hall, 2013), Cretaceous magmatism (Williams et al., 1988; Davies et al., 2014; Hennig et al., 2017), and volcanism during the Cretaceous (van Gorsel, 2012) to the Miocene (Williams and Harahap, 1987; Prouteau et al., 2001). Previous studies have correlated the tectonic activity with two main deformations namely, the NE-SW to NW-SE trending syn-depositional growth faulting during the Cretaceous-Eocene, superposed by the Late Miocene to the Pliocene NE-SW trending wrench-induced compressional folds (Shuib, 2003). However, Borneo has had very complex Cenozoic tectonics with extension; uplift and subsidence of different regions and rotation which has been subject to diverse interpretations by many authors (see Hall, 2013 and discussion within). In

addition, several basement faults and their frequent reactivation until the Pliocene-Pleistocene (Mat-Zin and Tucker, 1999) are thought to have played a significant role in the evolutionary history of the region. Within this regional tectonic framework, in addition to the West Borneo basement, the Sarawak region consists of three zones, from south to north: the Kuching zone, the Sibu zone and the Miri zone, which are distinguished based on stratigraphy, depositional environments and structural trends (Haile 1974). The three zones identified in the geological classification of Sarawak can be applied to the tectonics and structural zonation as well (Cullen, 2014; Mathew et al., 2016b). The Lupar Line (Fig. 1A) separates the Kuching zone and Sibu zone. It is interpreted as a strike-slip fault and this line would have probably reactivated several times until the Eocene times (Mat-Zin, 1996). The Sibu zone covers the area between the Lupar Line and the Bukit Mersing Line (Fig. 1A), which has been interpreted to be of a strike-slip nature (Mathew et al., 2016b) and active during the Eocene to the Middle Miocene. The Line was reactivated several times and this reactivation along with other movements led to an intense deformation in parts of central and north Sarawak (Mat-Zin, 1996). The Miri zone covers the area to the north of the Bukit Mersing Line. The central Sarawak region is an arcuate fold and thrust belt, commonly referred to as the NW Borneo Rajang Group fold-thrust belt. It extends along strike over a distance of ~1000 km and has a width of over 300 km (Tan, 1979; Williams et al., 1986; Tate, 1991; Hutchison, 1996; Moss, 1998). In central and north Sarawak, structural trend lines run in broad curves. The folds are interpreted to be tight, overturned and broken by thrust faults. The surficial topography of central Sarawak varies from terrain underlain by recessive shale through zones of linear ridges (interbedded sandstone and shale) to rugged highlands consisting of thick massive sandstones (Light et al., 1994). In the interior of Sarawak, a wide swath of discontinuous plateaus built of Late Cenozoic volcanic and pyroclastic rocks dominate the landscape.

The Kuching zone is composed of a basement complex (Breitfeld et al., 2017; Hennig et al., 2017) of schists (Madon, 1999), Paleozoic-Mesozoic marine sediments, and Paleogene fluvial-marginal marine sediments (Tan, 1979, 1993; Haile, 1974; Hutchison, 2005; Breitfeld et al., 2014). Several small post-basement intrusions of the Late Oligocene to the Miocene age cut through this zone. The Sibu zone consists of a highly deformed, steeply dipping, Belaga Formation (Liechti et al., 1960; De Silva, 1986; Hutchison, 2005) that consists of thick, monotonous sequences of shale and sandstone of deep marine turbidities (Bakar et al., 2007) deposited on the oceanic crust without any basement rocks (Kirk, 1957, Wolfenden, 1960; Haile, 1974). Based on $^{39}Ar/^{40}Ar$ dating, Cullen et al., (2013) reported the Upper Miocene-Pliocene age for the volcanics of Hose Mountain and ~4 Ma and 2 Ma for the bimodal volcanic rocks of the Usun Apau Plateau. The Miri zone is dominated by fluvio-

tidal to inner neritic marine shelf conditions upon an older continental crust (Haile, 1974; Madon, 1999; Hutchison, 2005).

Among these three zones, the low-lying coastal plain between the Gigis River in Mukah and the Lemai River in Balingian in the Miri zone in northern Sarawak, covering an area of ~710 km^2 (Fig. 1) forms the present study area. The Balingian province is bounded by the central Luconia province in the north, the west Balingian line in the west and the Tinjar province in the south (Wan Hasiah, 2003). Lithostratigraphically, the Mukah-Balingian sector consists of coal hosting fluvio-tidal sediments belonging to the Upper Miocene and the Pliocene age and the Quaternary alluvium and coastal forest-swamp peat (Anderson, 1964). The Miocene and the Pliocene sedimentary rocks consist of three formations (Wolfendren, 1960) namely (Fig. 2), the Liang Formation (Pliocene-Pleistocene), the Begrih Formation (Lower Pliocene) and the Balingian Formation (Upper Miocene). However, the age relations of these formations remain to be ascertained (Wolfendren, 1960). The Balingian Formation, deposited in lagoonal and estuarine environments, consists of clastic sediments (shale, mudstone, sandstone, and conglomerate) with interbedded coal and lignite, and is unconformably overlain by the Begrih Formation (de Silva, 1986). The conglomerate consists of inter beds of conglomerate, conglomeratic sandstone and coarse- grained sandstone with vertical and lateral variations, which are poorly sorted and crudely bedded (Sia et al., 2014). The angular unconformity between Balingian and Begrih formations is marked by Begrih Conglomerate, represented by a wedge of poorly sorted and crudely bedded conglomerate, conglomeratic sandstone and coarse-grained sandstone (Wolfendren, 1960; de Silva, 1986; Mat Zin, 2000). However, recognition of unconformity and differentiating the Balingian and Begrirh formations in the field are often difficult. Coal deposits in the region have been poorly dated. Occurrences of 12 coal seams reaching a total thickness of about 16 m (Sia and Wan Hasiah, 2011) were interpreted to have been deposited under warm and wet climatic conditions (Muller, 1972; Morley, 2010). Though the age of the Balingian Formation is assigned to be the Late Miocene, the younger Begrih Formation is comparable in age to the Miri Formation (Liechti et al., 1960; Wolfendren, 1960; Hutchison, 2005). Based on the abundances of *Casuarina* pollen associated with *Dacrydium, Stenochlaenapalustris, Florschuetzialevipoli* and *Stenochlaenaareolaris*, Sia et al., (2014) determined Early Miocene age to the Balingian Formation. It is comparable to the Zone PR9 of the palynological zonation of the Malay Basin. Based on the foraminiferal assemblages of the Balingian Formation, a brackish water depositional environment was inferred (Liechti et al., 1960; Wolfendren, 1960). Over the total thickness of 3000-3600m, only 1900m from the uppermost section is exposed in the study area. The Balingian Formation is recognized (Nugraheni et al., 2014) as containing gas-prone source (coals and organic-rich clays) and reservoir rocks (sandstones). The fluvial and non-marine Begrih Formation is

dominated by mudstone and less sandstone, conglomerate (ortho and sandy) and coal (de Silva, 1986; Nugraheni, et al., 2014) and is conformably overlain by the Liang Formation. The Liang Formation is underlain by the Begrih Formation in the north and by the Belaga Formation in the south (Hutchison, 2005). The depositional environments of the Liang Formation range from shallow marine in the north to coastal plain in the south. The geology, structure, stratigraphy and age of this region are still under discussion (for example, Hall and Breitfeld, 2017; Hall and Sevastjanova, 2012; Hall et al., 2008; Hall, 2012) and the regional geological description presented herein is only a synoptic review from the existing literature.

Fig. 2.

3. Material and methods

A systematic field survey was conducted near Mukah (Fig. 1B), to identify the occurrences of natural exposures and quarry sections. It was followed by the logging of well-preserved sections and further sampling. The regional geological map published by Hakimi et al., (2013) was utilized for a reconnaissance survey, then refined with field data and superimposed on the regional topographic map constructed with Shuttle Radar Topography Mission (SRTM) data and Google images (Fig. 1A, 1B). Three excellently preserved sections exposed in a coal mine were chosen for sampling. Rock-sediment (tephra), and coal samples from below and above the tephra layer were collected (Tephra samples from quarry: A, B, C; subsamples at bottom and top portions of tephra layer at A: A1, A2; coal samples from quarry: B Top, B Bottom). Another tephra sample (VA 37) from a core drilled at about 5 km away from the coal mine was also sampled. In addition, a reference ash sample from Mt. Pinatubo, Philippines (from Wards USA rock collections) was also analyzed for comparison.

The tephra samples were examined under reflected light microscopy, in the laboratory for macroscopic description and sub-sampling for granulometric, mineralogical, geochemical and radiometric dating analyses. Granulometric analyses of tephra samples from the quarry were performed with the help of a laser particle size analyzer erected at the Department of Geology, Lucknow University, India. The samples were treated with boiling H_2O_2 (10%) and HCl (1%) to remove organic matter and possible carbonates, respectively. The samples were then boiled with sodium hexametaphosphate ($Na_4P_2O_7 \cdot 10H_2O$) to ensure complete disaggregation of the particles, then subsequently introduced into the particle size analyzer. Size measurements made at every 10μm interval were consolidated at regular Folk and Ward's Phi (∅) scale and utilized for computing standard textural parameters namely, mean size (Mz), standard deviation (SD), skewness (S_K), and kurtosis (K_G) for characterization of the sediment types and inferences on depositional processes. All the tephra and coal samples were crushed and ground to pass through a 230 mesh (<63 μm size) for geochemical analyses. Thoroughly mixed and finely ground powders of these samples were utilized

for whole-rock mineralogical analyses using an X-ray diffractometer erected at the Birbal Sahni Institute of Paleosciences (BSIP), Lucknow, India and the resultant intensity-peak values were plotted and mineral species were identified using the standard powder data manual. Splits of the ground samples were utilized for whole-rock major, trace and rare earth elemental analyses. Whole-rock major, trace and rare earth elemental analyses were carried out at Actlabs, Canada. The fusion technique was employed using lithium metaborate/tetraborate for the major, trace and REE analysis. The resultant molten bead was rapidly digested in a weak nitric acid solution and the analyses was carried out by the ICP and ICP-MS. Certified reference materials NIST 694, DNC-1, GBW 07113 (for major and trace elements) and NCS DC70009, OREAS100a, 101a, and JR-1 (for REE) were used to calibrate the trace element concentrations during the ICP-MS analyses. Major oxide data were recalculated as anhydrous in nature and adjusted to 100%. Thin sections were prepared from sub-samples of each of the tephra samples and were examined under polarized light using a petrographic microscope for documenting the textural relationships and to identify sediment components. Smears of tephra samples were also examined under a reflected light microscope for nannofossils. The tephra samples and coal samples were examined for any occurrence of dinoflagellates. The tephra samples from the quarry were subjected to zircon separation and U-Pb dating and elemental analyses. Zircon separation from crushed rock samples was performed at the Yu'neng Geological and Mineral Separation Survey Centre, Langfang City, Hebei Province, China, using magnetic and density methods, followed by handpicking under a binocular microscope. The grains were mounted on an epoxy resin disk, polished to expose the internal texture, and then were examined under transmitted and reflected light. The intracrystal textures of zircons were studied under cathodoluminescence (CL) by using a scanning electron microscope (JSM510) equipped with a Gantan CL probe at the Beijing Geoanalysis Centre. Zircon U-Pb dating and element analyses were carried out on a Laser Ablation Inductively Coupled Plasma Spectrometer (LA-ICP-MS) housed at the National Key Laboratory of Continental Dynamics at Northwest University, Xi'an, China following the analytical procedures described by Yuan et al., (2004). In the LA-ICP-MS method, the laser spot diameter and frequency were 30 μm and 10 Hz, respectively. A standard zircon 91500 was used for the data correction and silicate glass NIST was used for optimization of the instrument. The raw data were processed using ISOPLOT 4.15 software (Yuan et al., 2004) and a common Pb correction was done using the method of Anderson (2002).

With these data generated from the field, petrographic, mineralogical, granulometric, geochemical and isotopic data, we assessed the probability of the occurrence of the tephra layer interbedded in thick coal seams. We then attempted the documentation of a past explosive volcanic event, the interpretation of the provenance of the sediments in the tephra layer and their

sedimentation process, and constrained on the regional tectonic events, the paleoclimatic conditions and finally examined the plausibility of the tephra layer being a marker bed.

4. Results

4.1. Field observations

The presumed tephra layer was found interbedded within very thick sub-bituminous coal seams which occur nearly all over the study area. Many large and active mines in the area have provided access to examine in detail the tephra layer occurrence in the field and permitted sampling. The coal seams are interbedded between the floodplain and the shallow-ephemeral channel sand deposits (Fig. 3), comparable to the present day monotonously featureless, coastal plains and swamps, drained by shallow fluvial channels. All over the studied and logged sections, the tephra layer appeared uniform in thickness (~6 cm), color (pale white) and compact, monotonous without any internal sedimentary structures (Fig. 3). Its lower and upper contacts were sharp, and without any transition. Similar characteristics were observable in the core sample recovered from the region, located about 5 km away (Fig. 1B) from the sampled mine section (Fig. 1B; Fig. 3).

Fig. 3.

4.2. Granulometry, petrography and mineralogy

Granulometrically, the tephra samples were bimodal, very poorly sorted, very fine - fine silt sized, very coarse skewed - very fine skewed and very platykurtic - platykurtic class. The tephra samples appeared translucent to isotropic under polarized light. They were mudstones showing a matrix supported nature in which cryptocrystalline, angular, fine silt sized glass shards (Fig. 4) were abundant. The X-ray diffraction data revealed a predominant proportion of kaolin with subordinate quantities of quartz and glass in all the samples (Fig. 5).

Fig. 4.

Fig. 5.

The zircon grains taken from three samples (A, B, C) were predominantly dark brownish in color except a few that were very dark, and a few other colorless and transparent grains. The majority of the grains were euhedral to anhedral in shape while prismatic to stumpy morphologies were visible in a few grains. Sizes of the grains ranged from 20-150 X 30-80 μm with aspect ratios of 3:1-1:1. A gradual increase in the sizes of the largest grains was observable in samples A, B and C. Many grains showed oscillatory zoning, patchy zoning or sector zoning under cathodoluminescence (CL) imaging. A few grains displayed core-rim textures. A few of these characteristics are depicted in Fig. 6.

Fig. 6.

4.3. Whole-rock major, trace and rare earth elemental geochemistry

The tephra layer samples showed high loss of Ignition (Table. 1) whereas, the coal samples collected from above and below location B (Fig. 1B; Fig. 3A) contained LOI which was more than half of their weight. The carbonate contents of the tephra samples ranged from 14-16 wt. % and inter sample variations of organic carbon and inorganic carbon contents as well. The results from the major, trace and rare earth elements (REE) analyses of the tephra samples including a reference volcanic ash sample from Mt. Pinatubo, the Philippines are presented in Table.2. All the samples were SiO_2, and Al_2O_3 dominant. In addition, higher Al_2O_3, and TiO_2 and lower Fe_2O_3, MnO, MgO, Na_2O, and CaO contents compared to the Upper Continental Crust (UCC; McLennan, 2001) were observed. Significant variations in elemental contents were also observed between the quarry and core tephra layers. The tephra samples from the quarry were argillized and characterized by a higher content of Al_2O_3 (average 35 wt. %) compared to the core sample (20 wt. %). The core sample was characterized by higher contents of SiO_2, Fe_2O_3, MgO, K_2O, and TiO_2 compared to the quarry samples. Tephra samples from the quarry section showed higher levels of Al_2O_3/TiO_2 (51 to 91; average: 65) compared to the core sample (Al_2O_3/TiO_2 = 20). Normalized elemental concentrations of tephra layers compared to the primitive mantle were analogous to tephra from Mt. Pinatubo, the Phillippines (Reference sample). As the tephra layers are highly susceptible to weathering (Dessert et al., 2009; Bottini et al., 2015) in which bulk dissolution is common (Cochran and Berner, 1996), study of relatively immobile elements for characterization and fingerprinting is preferred. The core sample contained higher concentrations of Sc, Be, V, Ba, Y, Zr, Cr, Co, Cu, Ge, Rb, Nb, Cs, Hf, Ta, Tl, Th, U, REE and lower concentrations of Ga and Pb compared to the quarry samples (Fig. 7). While the Zn, W, and Sr contents were relatively similar between the quarry and the core samples, significantly lower Rb, Nb, Sn and Cs in the quarry samples compared to the core sample were perceptible. The core sample showed higher concentration of these elements compared to the UCC and tephra from Mt. Pinatubo. Whereas, all trace elements showed lower concentrations than those of the UCC and the Mt. Pinatubo tephra samples, except for Pb, Th, and U. The chondrite normalized REE plots of the quarry samples showed light REE (LREE) enrichment, heavy REE (HREE) depletion and negative Eu anomaly. However, the core sample showed similar trend as of the Mt. Pinatubo sample, except for the Eu anomaly. The tephra layers had total rare earth element (∑REE) contents of 6-114 ppm (in quarry samples) and 223 ppm (in core sample) and were characterized by LREE enrichment relative to HREE with La/Yb$_N$ ratios of between 2-48 and 11 in the quarry and the core tephra layers, respectively. All the studied samples showed negative Eu/Eu* anomalies (0.55 to 0.68).

Table.1.

Table.2.

Fig. 7

4.4. Zircon geochemistry

Trace elemental compositions (Table.3) and U-Pb were determined on the zircon grains from selected spots. The twenty three spots of zircon grains in sample 'A' showed high and variable ∑REE contents ranging from 354-3229 ppm and Y contents varied from 383-4468 ppm. Their $(La/Sm)_N$ ratios ranged from 0.002-1.6 and $(Gd/Yb)_N$ ratios ranged from 0.024-0.08. The REE patterns showed a steep slope from LREE to HREE with positive Ce anomaly and a negative Eu anomaly, (Fig. 8). Nineteen zircon spots from sample 'B' mostly showed high ∑REE contents ranging from 508-1521 ppm and Y contents in the range of 578-2224 ppm with $(La/Sm)_N$ and $(Gd/Yb)_N$ ratios between a range of 0.002-0.423 and 0.024-0.077, respectively. Their REE patterns displayed a steeply-rising slope from LREE to HREE together with a positive Ce anomaly and a negative Eu anomaly (Fig. 7). Seventeen zircon spots from sample 'C' showed high ∑REE and Y contents of 191-2065 ppm and 237-3117 ppm, respectively. The $(La/Sm)_N$ and $(Gd/Yb)_N$ ratios showed ranges of between 0.0009-0.7137 and 0.0313-0.0782, as well as HREE enrichment, positive Ce and negative Eu anomalies.

Fig. 8.

4.5. Zircon U-Pb dating

Forty three, 38 and 37 spots were analyzed with their respective number of zircon grains from samples A, B and C, respectively. The results are presented in Figs. 9a, b, c, d, e, f. In sample "A", excluding 20 discordant spots, the remaining 23 spots were divided into three groups. One group included three older zircons with Th, U contents and Th/U ratios of between 90-176 ppm, 1707-359 ppm, and 0.34-0.76, respectively. They yielded Mesoproterozoic to Neoproterozoic ages of 1174 Ma, 1092 Ma and 791 Ma with high concordance. The second group included three spots with Th, U contents and Th/U ratios of between 88-810 ppm, 174-926 ppm and 0.51-1, respectively. They yielded the Carboniferous to Permian $^{206}Pb/^{238}U$ ages of 343 Ma, 318 Ma, and 280 Ma. The third group was the main population in this rock, and was composed of seventeen zircon spots with Th, U contents and Th/U ratios with ranges of between 77-761 ppm, 122-1774 ppm and 0.29-0.92, respectively. They yielded a weighted mean $^{206}Pb/^{238}U$ age of 11.48 ± 0.26 Ma (MSWD = 2.9, n = 17) (Fig. 9a, b). In sample "B", excluding twenty two discordant spots, the remaining sixteen spots with high concordance were divided into two groups. The first group was composed of five zircon spots representing xenocrysts with Th, U contents and Th/U ratios of between 88 to 272 ppm, 200-388 ppm and 0.44-0.71, respectively. They yielded a wide range of $^{206}Pb/^{238}U$ ages, from 456-74 Ma. The second group was the major population and included eleven spots that showed Th, U contents and

Th/U ratios of between 54-925 ppm, 81-1529 ppm and 0.36-0.91, respectively. They yielded a weighted mean $^{206}Pb/^{238}U$ age of 11.44 ± 0.37 Ma (MSWD = 2.4, n = 11) (Fig. 9c, d). In sample "C", excluding seven discordant spots, fifteen spots were divided into three groups. The first group was composed of three magmatic zircons with Th, U contents and Th/U ratios showing a wide range of between 77-282 ppm, 133-829 ppm and 0.34-0.58, respectively. They yielded Paleoproterozoic to Mesoproterozoic ages of between 2198-1249 Ma. The second group contained five spots with Th, U contents and Th/U ratios in the range of between 79-244 ppm, 172-509 ppm and 0.15-0.89, respectively. They yielded a wide range of ages from the Cambrian to the Cretaceous (533-80 Ma) suggesting the presence of older basement. The main concordant group included seven spots with Th, U contents and Th/U ratios of between 76-448 ppm, 117-978 ppm and 0.45-0.65, respectively. They yielded a weighted mean $^{206}Pb/^{238}U$ age of 11.76± 0.76 Ma (MSWD = 2.0, n = 7) (Fig. 9e, f).

Fig. 9.

5. Discussion

5.1. Volcanic origin of the tephra layer

The volcanic rocks, volcanoclastics (Reuter et al., 2012), tephra beds (Shen et al., 2013), and glass shards (Albert et al., 2015), among others provide geological archives to trace past magmatic events. Once the prevalent volcanic event(s) has been ascertained, a variety of tools and methods help recognize the proximity of the volcanic event with reference to the location of these archives. For example, while the volcanic flows/trap rocks are considered to accumulate in the immediate vicinity of volcanic events/vents/fissures, and the bombs and lapilli are considered to be deposited at a somewhat further distance. The thick tephra beds, thin tephra beds, admixture of ash and glass shards in sediments are considered to be located the farthest from the location of eruption. Recently, the cryptotephra, i.e., non-visible tephra (Albert et al., 2015; Tomlinson et al., 2015) or dispersed volcanic ash were recognized (Scudder et al., 2016; Tomlinson et al., 2015) through geochemical analyses of archives located more than 7000 km away from the location of the magmatic event. In this regard, the conspicuous lateral continuity with monotonously uniform color and thickness of the presumed tephra layer has covered a few kilometers despite its limited thickness (as reported by Stollhofen et al., 2000). Similarly, small and uniform grain sizes (mud-fine silt-muddy sand), together with angular, poorly sorted grains and with typical glass shards in the tephra bed typify prevalent distal, major volcanic events and subsequent atmospheric fallout of ash has been preserved between the coal seams of coastal swamps. The thickness of the tephra layer (~6 cm) suggests a large volcanic event whereas, tephra layers of >10 cm are considered the results of a very large volcanic event (Lowe, 2011; Fontijn et al., 2015). Additionally, absence of any internal sedimentary structures (physical, chemical and biological) within this layer supports the

interpretation of a short-duration deposition, and significant post-depositional compaction. The contact relationship (Fig. 3A) between the coal seams and the tephra layer, among others also testifies to the disruption of organic matter accumulation due to the influx of tephra from flood waters as well as atmospheric fallout and the resumption of organic matter accumulation (Fig. 3A; Table 1) after the tephra deposition. It also suggests the distal nature of the volcanic event that did not affect the vegetation and depositional environments of the coastal swamps directly. The predominantly siliciclastic and kaolinitic nature of the sediments of the tephra layer (also evident by the high LOI of all the tephra samples – Table 1), in which abundant volcanic glass shards and zircon grains typical of volcanic and magmatic origins are embedded, suggest a part of the sediments were recycled from paleosols and the immediate atmospheric ash fallout. Both of these underwent diagenesis/weathering in the new depocenters. The relative stability of kaolin compared to other clay mineral species even during climate shifts to drier conditions (Do Campo et al., 2010) could explain the predominance of kaolin in the samples. The CIA (chemical index of alteration) values ranged from 99.5 to 99.6 for the tephra layer of the quarry section, and 81 for the tephra in the core sample, indicating all the tephra samples were altered intensively. Though weathering and burial diagenesis alter the volcanic ash that could have released many elements (Christidis, 1998) into diagenetic fluids, the incompatible elements such as Ti, Y, Zr, Hf, Nb, Ta, Th and REEs are relatively retained and commonly not released (Christidis and Huff, 2009). Thus, it may be construed the immobile elements in the studied ash samples provide reasonably accurate information on the provenance and tectonic setting.

When volcanic ash falls onto non-marine coal forming environments and alters to kaolinite, it is termed tonstein (Addison et al., 1983). These tonstein beds are now universally accepted as volcanic in origin (Bohor and Triplehorn, 1993; Demchuk and Nelson-Glatiotis, 1993; Burger et al., 2002). The dual sources for the sediments is further ascertained by the distribution of the size class of the sediments (Fig. 10) which shows typically a bimodal nature, wherein the silt sized detrital grains and clay probably originated from recycled paleosols and *insitu* weathering products of volcanic ash. Occurrences of coastal swamp-lake-ephemeral fluvial inlets might have provided ideal accommodation space (Lowe, 2011; Fontijn et al., 2015) for these recycled sediments and atmospheric ash fallout. The glass shards are all angular and isotropic without exception (Fig. 4) suggestive of a wind-blown nature rather than transported by an aquatic medium. Or, even when partial contribution from a suspended mode of transport by an aquatic medium is assumed, absence of attrition is assumed.

Fig. 10

5.2. Geochemical provenance signatures

The geochemical and mineralogical signatures of siliciclastic and volcanoclastic sediments from different parts of the world are used to infer the source rock composition, climate, mode of transport, depositional environment, degree of source rock weathering, tectonic setting and post depositional processes such as diagenesis and metasomatism (McLennan et al., 1993; Burger et al., 2002; Kiipli et al., 2007; Do Campo et al., 2010; Nagarajan et al., 2014; 2017). The geochemistry of zircon is closely related to its parental magma composition and is effective for fingerprinting tectono-magmatic provenance (Grimes et al., 2015). Incompatible trace elements generally survive weathering and diagenesis and preserve original geochemical signatures of the host sediments/rocks. However, many chemical fingerprinting attempts have provided only mixed success (Christidis, 1998) in discriminating precursors/original signatures. Given cognizance to these, an examination of the steep slope (from LREE to HREE) of the REE pattern of zircon grains could suggest igneous affinity (Hoskin and Ireland, 2000), whereas the strong REE fractionation and negative Eu anomaly support a volcanic origin and an arc related magmatic source rock (Pearce and Peate, 1995). According to Shen et al., (2012, 2013), the single best proxy for volcanic ash content at Xinmin is Eu/Eu*, especially very low values of Eu/Eu* (0.2–0.8). Our data also fall within a very narrow and low range (0.52-0.68) signifying volcanic origin of the presumed tephra layer and an absence of significant differentiation either during emplacement and/or during sedimentation. The geochemical signatures of tonsteins are the results of many factors such as original ash composition, depositional environment and diagenesis (Burger et al., 2002), which, necessitate careful examination of the major oxide content for geochemical fingerprinting. Higher concentrations of SiO_2 in the studied tephra samples (Table 2) may indicate silicic volcanism as well as inputs from older continental material (Huang et al., 2016), recycling of older regolith, etc. It essentially suggested a dual mode of sediment sourcing, an inference made through sedimentological and mineralogical characteristics. The zircons from the tephra samples showed varied ages suggesting a mixture of detrital zircons in addition to the magmatic zircons according to their morphological (Fig. 6) and geochemical (Table 3) characteristics. This observation affirms dual provenance for the sediments in terms of detrital influx of clays from *insitu* weathering in the basement source areas and diagenetic alteration of tephra that settled at the depocenters. The existence of two groups of zircons (Fig. 9), one from the Late Miocene juvenile magma and another from the Paleoproterozoic-Cretaceous aged basement rocks and/or recycling of older magma during an eruption are inferred (detailed in the following section) which, in turn provides an affirmative evidence to the dual source for the tephra layer. The tephra samples showed a high Al_2O_3 content (Table 2) and contained a high proportion of kaolinite (Fig. 5). These could mainly be due to accumulation and humification of peat

layers under acidic conditions, which in turn were conducive to the diagenetic mineralization of kaolinite from the parent volcanic ash (Demchuk and Nelson-Glatiotis, 1993). It is likely the higher Al_2O_3 content is due to the conversion of tephra to authigenic silicate by the removal of other components such as SiO_2 and Na_2O (Kiipli et al., 2007). Also, coeval detrital input cannot be ignored since it might have modified the geological signal related to volcanism. Significant amounts of kaolinite in the tephra samples could have formed from hydrated Si-Al gels resulting from the volcanic glass hydrolysis (Bohor and Triplehorn, 1993; Liao et al., 2016). The tephra layer from the quarry section showed the SiO_2/Al_2O_3 ratio in the range of 1.17-1.20 (average. 1.18) which is comparable to the theoretical value for kaolin (1.18; Burger et al., 2002). However, the tephra sample from the core showed a higher SiO_2/Al_2O_3 value (3.12), indicative of geographic variation of the modification process or their intensity, or both. Similarly, the TiO_2/Al_2O_3 ratios in the tephra samples from the quarry (0.011-0.020; average.0.016) were consistent with a silicic volcanic origin (<0.02; Addison et al., 1983). The tephra from the core showed a higher TiO_2/Al_2O_3 ratio (0.049) compared to the quarry and reference (fresh volcanic ash from Mt. Pinatubo) samples. High Al_2O_3/TiO_2 ratios for the quarry samples indicate a felsic volcanic source while the core sample with a Al_2O_3/TiO_2 ratio of 20 suggested intermediate volcanic source (3-8 for mafic; 8-21 for intermediate and 21-70 for felsic igneous rocks; Hayashi et al., 1997). It seems probable the Al_2O_3/TiO_2 ratios in the quarry samples were affected by intensive argillite formation and weathering (CIA = 80-100). The inference of a felsic nature of source is reinforced by Th/Sc vs. Sc plot (Fig. 11a) and the La/Th vs. Hf plot (Fig. 11b) where the quarry samples plotted near the felsic source whereas the core sample plotted near the UCC and PAAS indicating intermediate signature. The Ti/Th ratio is used to distinguish different igneous rocks (30-400 for acid; 400-1000 for intermediate and 2500-3500 for mafic volcanic rocks respectively; Feng, 1989). Accordingly, the Ti/Th ratios, in the range of 165-309, computed for the studied samples are indicative of a felsic igneous source, the high Th and U contents (Th>3 ppm and U>2 ppm) indicated intermediate- felsic origin. The intermediate to felsic source is also supported by the U vs. Th plot for zircon grains in which they are plotted in the Dacite to Rhyolite field while the cross plot of U/Th suggested continental and oceanic crustal origin for the zircons (Fig. 12).

Fig. 11.

Fig. 12.

The Th/U ratios and internal structures (Corfu et al., 2003) of these grains were consistent with magmatic crystallization (Hoskin and Schaltegger, 2003). This inference is supported by variable $\sum$ REE and Y contents (Table 3), suggesting the involvement of crustal material in the magma. Further, the HREE enrichment, together with positive Ce anomaly and negative Eu anomaly (Fig. 6c) are

typical of magmatic zircons. These magmatic zircons are similar to those of zircons from rhyolite and dacite (Fig. 12). This confirms that fine vitric and labile primary minerals from a distal rhyolitic source were deposited, and later diagenetically altered into kaolin by leaching alkaline and alkali earth metals under acidic fluids in the peat swamp.

5.3. Geochemical signature of tectonic setting

Bulk chemistry based tectonic discrimination plots proposed by Roser and Korsch, (1986) demonstrated the utility of whole-rock geochemistry in discriminating the tectonic setting of sediments. Taking cues from this work, Verma and Armstrong-Altrin, (2013) proposed two new tectonic discrimination diagrams for siliciclastic sediments derived from island/continental arc, continental rift and collision. The same methods were attempted for the tephra samples under study. The tephra samples from the quarry section were plotted in the low silica region and the core and reference samples were in the high silica region (Fig. 13a, b) suggestive of collisional and arc tectonic settings, respectively. The Discriminant diagrams of Roser and Korsch (1986) also indicated similar tectonic settings for the quarry samples (Fig. 13c, d) whereas the core sample was plotted in a passive collisional tectonic setting. Together, these observations may signify the dual sources of sediment influx, regional variation of sediment characteristics as well as limitations of discriminant diagrams. However, the general affinity of tephra with rhyolitic composition has been interpreted by Shen et al., (2012) to be in a volcanic arc tectonic setting in a subduction zone, consequently, the collisional and arc settings suggested by the discriminant diagrams of Verma and Armstrong-Altrin, (2013) could be considered valid. This inference is further substantiated by the $\sum$REE and Y contents (Table 3), the HREE enrichment, and the positive Ce and negative Eu anomalies (Fig. 8c) of the zircon grains, which suggest rhyolite and dacite composition of the parental magma (Fig. 12).

Fig. 13.

Owing to the significantly altered nature of the tephra layer as indicated by the CIA values, the inferences on tectonic settings based on the major oxides and mobile elements become circumspect. In order to circumvent this complexity, the incompatible trace elements based discrimination diagrams such as Y vs. Nb and Yb vs. Ta were used (Pearce et al., 1984). In the Yb vs. Nb diagram (Fig. 13e) all the studied tephra samples including the reference sample (v.ash from Mt. Pinatubo) plotted on the volcanic arc and the syn-collision granite field. Similarly, in the Yb vs. Ta diagram (Fig. 13f) the tephra samples from the quarry section plotted on the volcanic arc granite field whilst the tephra core sample and reference sample plotted on the ocean ridge granite field. The VAG character of the ash samples were comparable to the results of Macpherson et al., (2010) and Cullen et al., (2013) who determined most magmatic rocks in Borneo had VAG character due to

their origin (melting of old arc material). In addition, the absence of affinity with ARC could also be inferred.

Tectonic collisions between island arcs, island arcs and continents, continental fragments, and volcanic arcs surround the Sundaland region to the east, west and south, where the lithosphere of the Indian and Pacific Oceans is subducted at high rates, accompanied by severe seismicity and volcanism. The region underwent southward-directed subduction under West Borneo during the Triassic-Cretaceous (Hennig et al., 2017; Breitfeld et al., 2017). Furthermore, during the Late Cretaceous, this subduction process formed the Schwaner Mountains (Williams et al., 1988; Davis et al., 2014; Hennig et al., 2017), which ceased at about 90-80 Ma (Clements et al., 2011; Hall, 2013; Davies et al., 2014; Breitfeld et al., 2017; Hennig et al., 2017). However Hutchison et al., (2000) suggested this subduction event might have lasted until 60 Ma. The Lupar Line, presumed previously to be the trench/suture (Clift et al., 2008) is considered a younger strike-slip fault. Much of the geology witnessed now is largely the outcome of Cenozoic subduction and collision at the margins surrounding the continental core of Sundaland (Metcalfe, 2011), which is situated at the boundaries of three major plates (Hall, 2009): Eurasia, India–Australia and Pacific–Philippine Sea (Fig. 1A). At the beginning of the Cenozoic, large-scale tectonic activities commenced in the western segment of Sundaland with the collision of India–Asia during the Eocene (Ali and Aitchison, 2005; Leech et al., 2005; Aitchison et al., 2007). At ~45 Ma, Australia began to move rapidly northwards, resuming subduction at the Sundaland margins, initiating an active margin on the south side, forming the Sunda Arc where there has been continuous subduction of ocean lithosphere beneath the Arc since the Eocene (Fig. 1A). This subduction also gave rise to an active margin in Borneo, and a volcanic arc that ran the length of Java accompanied by widespread intense volcanism in regions between Sumatra and Sulawesi (Crow, 2005). There have been alternative interpretations as well: During the Eocene and the Oligocene, from Sumatra to Sulawesi, abundant volcanic activity accompanied northward subduction of the Indian–Australian Plate. The Cenozoic magmatism has been considered a complex event with diverse opinions on the timing and origin of the event (Williams and Harahap, 1987; Prouteau et al., 2001; Cullen et al., 2013). During the Late Cretaceous–Early Eocene, rifting at the margin of Asia to produce the South China Sea took place, resulting in a southward movement of the Luconia continental block that led to the conception of a magmatic belt due to the southward subduction. The Lupar Line (Fig. 1A) coincides with the Late Cretaceous subduction trench. In the Early Miocene, a collision in Borneo with the extended continental margin crust of South China has been documented as giving rise to magmatism in central Borneo, but volcanic activity largely ceased after the collision (Hutchison et al., 2000; Hall, 2009). However, based on precise age data on the basaltic plateaus, Cullen et al., (2013) have questioned assigning the Early Miocene age to this

collisional event and the magmatic events that followed. In the Java–Sulawesi region, volcanism diminished during the Early and Middle Miocene although in Sumatra, volcanic activity was apparently continuous with a period of reduced activity only during the Late Miocene. In Borneo, a Tertiary magmatic arc ran from northeast Kalimantan southwards through Central and West Kalimantan to Sarawak, following the southern boundary of the Kuching High (Carlile and Mitchell, 1994). Along this magmatic arc, three magmatic episodes have been identified: the Eocene acidic volcanism followed by the Late Oligocene-Miocene andesitic-rhyolitic volcanism and then by the Plio-Pleistocene basalt volcanism (Soeria-Atmadja et al., 1999). In the interior of Borneo, along the border of Sarawak and Kalimantan, plateaus of Cenozoic lavas and pyroclastic cones associated with a volcanic arc can be witnessed. They consist mainly of rhyodacites, andesites, basalts and calc-alkaline to potassic-calc-alkaline volcanics (Soeria-Atmadja et al., 1999). The K/Ar ages of these plateaus vary from 25 - 4 Ma and dacitic, ignimbrite tephras, glassy lavas and breccia are the vital products of this phase of volcanism (Cullen et al., 2013). Prouteau et al., (2001) reported ages of 6.4 to c. 22 Ma for adakites and diorites in Sarawak; although consensus on the ages and origin of those rocks has not yet been achieved. Given the geodynamic complexity of the Sunda region and the intense volcanism during the Cenozoic Era, our results could indicate magmatic activity during the latest Middle Miocene. While the aforementioned magmatism could be a reasonable explanation for our results, magmatic activity related to subduction in the Borneo-Palawan Trough (Fig. 1A) during the Middle Miocene–Pliocene, the Pliocene-Pleistocene intraplate magmatism in the southern Sulu Arc (Macpherson et al., 2010) as well as ongoing explosive volcanism in neighboring Sumatra and the Java–Sulawesi sector cannot be ignored. In this regard, an accurate pinpointing of a volcanic event and its duration are essential, and are presented in the following section.

5.4. Age and implications on stratigraphic marker

Explosive volcanic eruptions are responsible for the widespread dispersal of ash (particle diameter <2 mm) or tephra. The near instantaneous deposition of tephra in geographically wide areas promotes formation of stratigraphic markers in a range of sedimentary records (Kilian et al., 2003; Bertrand et al., 2014; Tomlinson et al., 2015). These markers are often useful for precise stratigraphic classification and correlation (tephrostratigraphy) of archaeological, lacustrine, peat and marine archives. If absolute age of the tephra is known from an independent numerical dating method, then the tephra horizons provide age markers within the stratigraphy (tephrochronology). Where a tephra can be attributed to a specific eruption of known age, it can serve as a chronological marker (Donato et al., 2016). Tephrochronology plays a critical role in refining age models in paleoenvironmental records and the synchronization of those records in order to determine leads and lags of rapid climate changes (Tomlinson et al., 2015). Key tephrostratigraphic markers rely upon

a widespread dispersal from a volcanic source with their chemical and petrographic fingerprints being well characterized, which enables the identification of diagnostic features unique to individual eruptions.

In this regard, the documentation of a monotonously uniform tephra bed, interpreted to have originated from a volcanic source, based on petrographic, mineralogical, and geochemical characteristics and occupying a geographically large area, and possessing similar characteristics, provides ample scope for its use as a stratigraphic marker at a regional scale. This is particularly important in the Sarawak region, both onshore and offshore, should this bed be encountered and the host sequence needs to be correlated. A *priori* requirement for this purpose is a precise and narrow range of radiometric ages for the zircon grains. In this regard, the presence of zircon grains yielding a discordant age group ranging from the Proterozoic-Late Miocene, in all the samples requires an explanation. A similar age group (1300-2440 Ma: Meso-Paleoproterozoic) was reported for the detrital zircons from the Miocene sediments from NW Borneo (Nagarajan et al., 2017). Other independent studies in the region have also reported similar discordant age groups (for example, van Hattum, 2005; van Hattum et al., 2006, 2013). Inheritance of zircon grains from older rocks has also been reported in many previous studies including Breitfeld et al., (2014; Cenozoic sediments of the Kuching Zone), Breitfeld et al., (2017; from clastic Triassic Sadong and Kuching formations and the Cretaceous Pedawan Formation in the Kuching Zone), Hennig et al., (2017; from granites in SW Borneo and the Kuching Zone) and Galin et al., (2017; from the Rajang Group in the Sibu Zone). The study area has been the loci of significant plate tectonic reorganization and magmatic, volcanic, climatic and topographic dynamics. The zircon grains studied display features typical of magmatic and volcanic origin. The xenocryst zircons found and measured for absolute age show a wide range of ages suggesting sediment influx from a variety of basement rocks ranging in age from the Paleoproterozoic to the Cretaceous. Alternatively, these older groups of zircons might represent xenocrysts mixed with the basement rocks during eruption. A consideration of xenocrysts of zircons and their recycling together with juvenile zircon crystals during a volcanic explosive event may explain the survival of the Paleoproterozoic-Cretaceous-Miocene magma chamber, and the effusive activity during the Late Middle Miocene along the inherited vent. A recent study by Cottam et al., (2010), reported the occurrence of the Cretaceous age zircon crystals in the Late Miocene Mount Kinabalu pluton, suggestive of the recycling of juvenile zircons from the magma chamber and the active nature of the chamber since the Cretaceous (Cullen, 2014). Geochronological data based on the SHRIMP (Sensitive High-Resolution Ion Microprobe) method of dating zircons from Borneo sandstones were presented by van Hattum (2005) and van Hattum et al., (2006, 2013). These studies have also reported the occurrence of zircons from multiple age-clusters, namely, the Eocene

(49.9±1.9 Ma) to the Archaean (2531.6±11.2 Ma), with the regional predominance of specific clusters belonging to the Cretaceous (~77–130 Ma), the Permian–Triassic (~ 213–268 Ma), and the Paleoproterozoic (~ 1750–1900 Ma). This is suggestive of inherited juvenile as well as recycled detrital zircon influx into the clastic sedimentary records of this region, including the tephra-lacustrine-fluvial plain deposits currently reported in the present study. Excluding the older xenocrysts, the data from the major zircon population in all three samples have consistently yielded weighted mean ages in the range of $^{206}Pb/^{238}U$ age of 11.44 ± 0.37 to 11.76 ± 0.76 Ma (Fig. 9) delineating the timing of the eruption. The difference between the lower and upper age limits of the ages of three tephra samples have suggested a duration of about 320 kyr as the period of eruption/volcanic activity. Nevertheless, zircon grains from all three tephra samples show the same age of eruption within error. Zircon SHRIMP data or/and Ar-Ar data on a larger suite of samples from different levels of the tephra layer in additional locations are required to precisely determine the duration of the eruption.

5.5. Implications on paleoclimatic conditions

An independent, triple examination of the tephra samples for the presence of palynoflora and dinoflagellates proved to be negative. Despite having been deposited in a lacustrine-swamp-coastal plain setting and luxuriant vegetation that formed very thick coal seams (refer Fig. 3A and the litholog inset and discussion in the following section) and the presence of a sandwiched tephra layer, palynologically barren samples may indicate the frequency and intensity of the eruptions as well as an extreme climate and or diagenesis. A similar barren nature due to the prevalence of detrimental climatic conditions and destructive geological events were reported previously elsewhere (e.g., Williamson and Bell, 2012). Ward (2009) demonstrated a direct connection between the frequency and the intensity of global magmatic activity and episodes of warming and cooling, principally driven by the quantum of SO_2 released during volcanic activity. Volcanic ash-fall events caused additional stress to the biota in tectonically active regions (Reuter et al., 2012), through a variety of after- effects including, but not limited to, thermal impedance, acid rain, alteration of the photic zone, and the enhanced turbidity in aquatic systems (Reuter et al., 2012). However, owing to their fine grain size and chemical reactivity (Dessert et al., 2009), ash particles also served as nutrients to aquatic systems (Reuter et al., 2012). Volcanic ash deposited in the aquatic systems affects oxygen diffusion into the underlying sediment, causing the formation of dysoxic/anoxic pore-waters (Perrier et al., 2012). Set on an active tectono-volcanic-magmatic landscape, the rocks that existed in the region might have experienced accelerated rate of weathering. This may have been primarily induced by their proximity to a volcanic setting, as volcanism is also a source of acidity (Keller and Lehnert, 2010) either through the emission of gaseous CO_2, H_2S or SO_2 (Ward, 2009;

Keller and Lehnert, 2010) or, to a lesser extent, HCl and HF or through the leaching by rainwater of volcanic gases in ashes. This excess of acidity characterizing volcanic regions might be concentrated in the local atmosphere. According to Dessert et al., (2009), in volcanic areas, natural acids that react with silicate minerals are not limited to carbonic acid. Important contributions also come from sulphuric and hydrochloric acids resulting from volcanic degassing, oxidation of reduced sulphur minerals (pyrite) and H_2S gas, and leaching of volcanic ashes. These conditions might have encouraged tephra to alter rapidly, which then became highly susceptible to alteration due to its crystallinity and high surface area to volume ratio (Dessert et al., 2009). Susceptibility to weathering of rocks rich in glass was reported by Cochran and Berner (1996), which suggested lithologically favorable conditions, in addition to atmospheric and geomorphic factors for the inferred significant weathering prior to and immediately after the explosive volcanic event. If so, it is highly probable the palynofossils and dinoflagellates that were washed from basement regions and deposited together with the tephra might have also been destroyed during an intensive alteration of tephra.

Consideration of sediment influx from weathered profiles of older basement rocks requires climatic milieu conducive for chemical weathering prior to the volcanic event, followed by erosion, transportation and deposition during and immediately after the event, and then deposited together with atmospheric ash fallout. Otherwise, catastrophic flooding (Williamson and Bell, 2012) and widespread erosion in catchments areas that previously supported extensive development of regolith over basement rocks and remained hitherto uneroded need to be assumed. If the latter is true, the factors that contributed toward the enhancement of erosional susceptibility need also to be unraveled. It is generally accepted major volcanic events significantly alter the atmospheric circulation and chemistry, in addition to promoting catastrophic rain fall (Williamson and Bell, 2012) and a similar scenario is considered plausible in the present study, which in turn could explain the sudden and enhanced erosion and the influx of detrital sediments immediately after the volcanic event. Previous studies (van Hattum, 2005; van Hattum et al., 2006, 2013; Nagarajan et al., 2017), available data from the present study, tectonic history and the depositional model discussed (following section) all suggest the existence of older basement rocks that were eroded to supply detrital sediments and were deposited in the peat swamps together with atmospheric fallout. Occurrences of many basement faults and their frequent reactivation until the Pliocene-Pleistocene were reported (Mat-Zin and Tucker, 1999) to have played significant roles in the evolutionary history of the region. These authors have also reported a major non-conformity in the regions offshore and have assigned the Serravillian, ranging from 13 to 11.5 Ma, falling within the radiometric dates obtained by the present study. This suggests deposition of sediments eroded from older basements by the lacustrine and coastal plain environments and cessation of offshore transport during this

time. Additionally, the time span coincides with a sharp sea level rise, perhaps, coeval with or resultant due to the enhanced volcanic activity. However, the short, sharp sea level rise (Mat-Zin and Tucker, 1999) was eustatic, according to the revised sea level curve of Haq et al., (1987). Therefore, it is plausible the volcanic event might have exacerbated the rise locally or regionally in terms of magnitude and rate, given the magnitude of the volcanic event based on the thickness of the tephra and the duration of the event.

While reviewing the regional geology of the region, Hall et al., (2008) stated the Early Miocene Nyalau Formation sandstones occupying a major part of the study area are compositionally mature sediments deposited under humid tropical conditions, and are considered to be recycled (based on their quartz-rich character) and derived mainly from the much older Rajang Formation. Both tropical weathering and acidic volcanic input can result in quartz-rich sediments that may be interpreted as mature recycled sandstones with a continental provenance. Consequently, this statement may be construed to support present observations and inferences on both counts, i.e., recycling of older sediments and volcanic inputs and the prevalence of requisite milieu conducive for deep weathering before a major volcanic activity produced the tephra layer. The interpretation of occurrences of thick regolith in the provenance of the present study area and the transport of kaolin or its precursor phases from the basement regions to the depositional site during and or immediately after the volcanic event necessitates an examination of the climatic conditions that favored enhanced and rapid chemical weathering (Ward, 2009). Volcanism may induce short-term (sub-decadal) atmospheric cooling, deplete ozone, and affect the hydrologic and carbon cycles. The climatic response to volcanism is similarly complex and difficult to predict, with the potential for global warming related to enhanced CO_2 emissions or regional lowering of albedo from tephra deposition on snow or ice, and for regional or hemispheric cooling due to aerosol radiation effects in the atmosphere or global cooling by tephra-fertilized marine CO_2 drawdown. Each of these processes occurs with its own characteristic timescale, and the type and degree of climate response is likely sensitive to the location, magnitude, composition, and climatic context of a given eruption. Furthermore, the relatively limited spatial extent of the macro-tephra fallout and the short-term nature of these events make it difficult to identify and link a geologic record of a climate response to a given volcanic eruption. Nevertheless, it is likely volcanism may be an important source of abrupt climate forcing, which may help to trigger instabilities in the climate system (Praetorius et al., 2016). Guo et al., (2008) opined that the global climate system experienced a series of drastic changes during the Cenozoic. In Asia, these changes include the climate transformation from a zonal pattern to a monsoon-dominated pattern that favored extensive formation of regolith profiles (paleosols) across the region during the Early Miocene that contributed sediments to younger deposits. While

examining the Aptian climatic conditions, Bottini et al., (2015) has suggested ash and gas injected into the atmosphere by subaerial volcanism may induce short-term cooling associated with individual degassing phases and the feedbacks of which may lead to atmospheric CO_2 drawdown via accelerated weathering. This mechanism perhaps fits well with the study area. The occurrences of multiple shallow channel-fill deposits (Fig. 3A) strewn all over the coastal-floodplain deposits overlying the coal seams, the sharp erosional contacts between coastal-flood plain and channel deposits, and the occurrences of kaolin as the dominant mineral in the tephra layer indicate, warm-humid climatic conditions (Do Campo et al., 2007). All of this has provided milieu conducive to the development of thick regolith over basement rocks, has rapidly weathered the ash-deposits, and was followed by flashfloods in the aftermath of a major eruptive event(s). Williamson and Bell (2012) also inferred similar climatic conditions and flash-flood events from the Palaeogene lava field of NW Scotland.

Praetorius et al., (2016) have suggested while direct radiative-forcing effects from individual eruptions are unlikely to lead to long-term cooling due to the relatively short residence time of volcanic aerosols into the upper atmosphere (1–3 yrs.), a prolonged increase in the frequency of eruptions could lead to either warming or cooling perturbations through ice-albedo, sea-ice, or CO_2 feedbacks. Modeling studies suggest hemispheric cooling for decades - centuries can be initiated by the effects of multiple eruptions, or sea-ice feedbacks. In the light of the presence of a dominant proportion of kaolin, followed by quartz and glass in tephra layer sandwiched between very thick coal – fluviatile sand deposits, a relatively significant and lengthy climatic perturbation occurred as a result of an earlier volcanic event that lasted approximately 320 kyr as delimited by the range of radiometric data (notwithstanding the analytical error limits).

5.6. Genetic and paragenetic model

Volcanogenic sediments form discrete beds when deposited by air fall, during and immediately after a large eruption. The components of these beds may consist of primary and secondary sediments originating from pyroclastic, epiclastic, and authigenic processes. An interpretation was made from the lithofacies characteristics (Fig. 3A) as documented in the exposures of quarry sections and core samples, regional geology and inferred paleogeomorphology, the prevalence of wide, gently sloping coastal plains, strewn with shallow ephemeral fluvial channels, and dotted with shallow fresh water lakes and extensive coastal swamps (Fig. 14a). In this regard, the inference of a sandwiched nature of moderately thick (~6 cm) tephra between very thick coal seams and predominantly fluviatile sandstones deposited in an extensive coastal plain-swamp depositional setting has certain implications, as the thickness of pyroclastic material reflects proximity of a volcanic source (Sowerbutts, 2000). Hall et al., (2008) interpreted proximity of a

volcanic source based on unabraded, euhedral zircon grains, akin to the present study and inferences. An absence of large pyroclastic material and the presence of a thick (~6cm) tephra deposit suggests a distal, yet very large volcanic event. The non-vesicular (glassy shards) and non-juvenile volcanic clast types (zircon xenocrysts of magmatic origin) found within the tephra layer, combined with the areal extent of the deposits and rhyolite-dacite nature suggest the material was supplied from a plinian eruption characterized by intense magma fragmentation. This has produced tephra together with a few crystals and these were expelled through the vent. Assuming the control of stratospheric winds with a present-day dispersal pattern (Do Campo et al., 2010), deflection of the plinian and sub-plinian eruption column occurred in response to a dominant stratospheric wind and promoted aeolian transport and dispersal of volcanic material of the size range of fine ash were interpreted and compatible with a distal source. The general distal nature of rhyolitic to dacitic pyroclastic components (Bertrand et al., 2014; Albert et al., 2015; Donato et al., 2016) supports the interpretation of the prevalence of a contemporaneously active Late Middle Miocene magmatic source from regions depicted in Fig. 15. Though the vicinity (Fig. 15) could suggest magmatism from the Mt. Kinabalu pluton as the source of the tephra, newly available U-Pb zircon dating of the Kinabalu pluton (Cottam et al., 2013) suggests the pluton is much younger (7.8-7.2 Ma) than our own age data of the zircons from the tephra samples ($^{206}Pb/^{238}U$ age of 11.44 ± 0.3711.76 -Fig. 9). There might have been an earlier phase of magmatism, but field evidence (surface or subsurface outcrops of rocks corroborating with this age limit) has been lacking or has yet to be documented. Alternatively, adakitic magmatism in West Sarawak and/or the Sulu arc in East Sabah could be considered as the source. In this regard, the tectonic setting interpretation of the tephra layers in terms of VAG, and the reports of Macpherson et al., (2010) and Cullen et al., (2013) consider most magmatic rocks in Borneo to be of VAG character. This lends credence to the interpretation of magmatic sources from West Sarawak and/or East Sabah as the provenance of the tephra layer analyzed in the present study. The geochemical characteristics of volcanoclastic sedimentary rocks may be directly related to their source as the concentrations of some elements (e.g., Ti, Y, Nb, Zr, Ta) remain fairly constant and undergo little modification despite susceptibility to changes due to transport mechanisms and mixing of materials from diverse source areas (Pinto et al., 2004). Owing to their similarity of the major elemental chemistry of rocks originating from multiple magmatic events but from the same source, often trace elements and REE rather than major elemental compositions are utilized for characterizing and fingerprinting tephra layers (Donato et al., 2016). In this regard, present observations on major, trace and rare earth elemental composition show a general affinity with felsic and specifically to rhyolite-dacite source magma suggests a single effusive volcanic source, and more importantly, a single major volcanic event rather than multiple events.

A predominance of kaolin and quartz with scattered glass shards and zircon grains in the studied samples, suggest dual provenances for the sediments: weathered regolith developed over paleoflood plain, and direct atmospheric fall-out of tephra. This inference reaffirms the interpretations of coastal plain-swamp-localized shallow lakes as the regional depositional setting (Fig. 14a), the deposition (Fig. 14b, 12c) of ash material from atmospheric fall out coeval with catastrophic flood-related detrital influx of weathered material from older basement, the prevalence of coal forming luxuriant vegetation prior to and after major volcanic eruption-tephra layer deposition (Fig. 14d) and its preserved tephra sandwiched between coal beds (Fig. 3). The facies association, sedimentological, mineralogical and geochemical characteristics of kaolinitic layers, originated from volcanic ash, and as described by the present study, largely agreed with the descriptions and characteristics presented by Fauret et al., (1996). These authors noted the tonsteins are compact, relatively thin (< 100 mm), kaolinitic rocks. They showed sharp contacts with overlying and underlying strata and often had considerable lateral extent, and commonly occurred in coal seams. There is now general agreement that most, if not all, tonsteins formed from the alteration of volcanic ash. Tonsteins that have formed from volcanic ash are usually thin, having formed over a relatively short time span. It may be that volcanic ash, possibly in addition to detrital kaolinite being deposited in a low-energy environment, was washed into the depositional sites. In addition, the volcanic material may have been reworked after deposition in the swamp because it is plausible organic material may be transported some distance, with only a negligible introduction of inorganic material, to form allochthonous peats – all of which fit precisely with the geological setting and depositional model.

Fig. 14.

Fig. 15.

Physical compaction, chemical and mineralogical alterations were also ensued. The peat-swamp environment is also characterized by a high content of organic carbon (Table 1; C_{Org} of tephra samples: 8.5-14 wt.%; coal samples: 46.8-52.4 wt.%; C_{Inorg} of tephra samples: 10-11.4 wt.%; coal samples: 6-6.5 wt.%) in the studied samples. The clay mineral assemblages were interpreted to be the result of a combination of a complex set of factors, such as source rock, climate, transport, and diagenesis. Occurrences of kaolinite is regarded as a product of the chemical weathering of feldspars and probably was removed from paleosols and paleoweathering profiles developed on coeval volcanic–volcaniclastic deposits and older volcanic and crustal rocks (Spalletti et al., 2008). It may also relate to the prevalence of enhanced humidity. The angular, bimodal-polymodal, poorly sorted and platykurtic characteristics of the sediment grains suggest deposition from a suspension cloud, short distance of transport and quick burial. Given the grain size, modality (Dix and Al-Dulami, 2011),

reactivity of the tephra and the environment of deposition and climate, it is perceivable the tephra underwent significant weathering, as reported elsewhere (e.g. He et al., 2010; Williamson and Bell, 2012). Thus, the sedimentological features suggest the volcanic material accumulated on the vast coastal swamps and plains by primary fallout processes and was later remobilized and redeposited together with fresh material. While the weathering profile development in the basement rocks of a detrital source region was aided by favorable climatic conditions, diagenetic alteration of deposited material was aided presumably by physical compaction by overburden, high reactivity of the tephra material to chemical alteration, and significant differences between the host rock and circulating fluids, emanating from associated coals beds.

6. Conclusions

Based on the occurrence of a tephra layer in geographically separated locations, yet with monotonously uniform sedimentological, petrographic, geochemical and chronological characteristics as detailed in this study, we have identified an explosive volcanic event that occurred between 11.44 - 11.76 Ma on a fairly a large scale that lasted for ~320 kyr. With the prevalence of monotonously horizontal, wide coastal plains with luxuriant coal-forming swamp vegetation, and associated shallow, ephemeral fluvial channels and a lacustrine depositional setting was interpreted. The tephra layer found sandwiched between very thick coal beds received detritus from atmospheric fallout after the explosive volcanism and erosion of regoliths that developed over older basement rocks. Significant perturbation of climatic conditions, the occurrence of a catastrophic flood following the explosive volcanic event and the restoration of the previous environmental and depositional setting were also revealed. Documentation of the genetic and paragenetic sequence of events, occurrences of a well-preserved tephra layer with monotonously uniform characteristics in geographically widely separated locations has provided ample scope for the bed to be used as a regional stratigraphic marker. Reporting the precise radiometric date in the present study and coeval of a sharp sea level rise in the relative sea level chart provide a perfect stratigraphic marker to correlate the terrestrial (lacustrine and coastal plain clastics) with offshore (prodelta and bathyl) equivalents.

References

Addison, R., Harrison, R.K., Land, D.H. and Young, B.R., 1983 Volcanogenic tonsteins from Tertiary coal measures, East Kalimantan, Indonesia. International Journal of Coal Geology 3, 1-30.

Albert, P.G., Hardiman, M., Keller, J., Tomlinson, E.L. Smith, V.C., Bourne, A.J., Wulf, S., Zanchetta, G., Sulpizio, R., Müller, U.C., Pross, J., Ottolini, L., Matthews, I.P., Blockley, S.P.E. and Menzies, M.A., 2015 Revisiting the Y-3 tephrostratigraphic marker: a new diagnostic glass geochemistry, age estimate, and details on its climatostratigraphical context. Quaternary Science Reviews 118, 105-121.

Ali, J. R., and Aitchison, J. C., 2005 Greater India. Earth Science Reviews 72, 169-188.

Anderson, J.A.R., 1964 The structure and development of peat swamps of Sarawak and Brunei. Journal of Tropical Geography 18, 7-16.

Anderson, T., 2002 Correction of common Pb in U-Pb analyses that do not report ^{204}Pb. Chemical Geology 192, 59-79.

Aitchison, J. C., Ali, J. R. and Davis, A. M., 2007 When and where did India and Asia collide? Journal of Geophysical Research 112, B05423, doi:10.1029/2006JB004706.

Bakar, Z.A.A., Madon, M. and Muhamad, A.J., 2007 Deep-marine sedimentary facies in the Belaga Formation (Cretaceous-Eocene), Sarawak: Observations from new outcrops in the Sibu and Tatau area. Geological Society of Malaysia Bulletin, 53, 35-45.

Bertrand, S., Daga, R., Bedert, R. and Fontijn, K. , 2014 Deposition of the 2011–2012 Cordón Caulle tephra (Chile, 40°S) in lake sediments: Implications for tephrochronology and volcanology, Journal of Geophysical Research Earth Surface 119, 2555-2573.

Bohor, B.F. and Triplehorn, D.M., 1993 Tonsteins: altered volcanic-ash layers in coal-bearing sequences. Geological Society of America Special Paper 285, 44p.

Bottini, C., Erba, E., Tiraboschi, D., Jenkyns, H.C., Schouten, S. and Damste, J.S.S., 2015 Climate variability and ocean fertility during the Aptian Stage. Climate of the Past 11, 383-402.

Breitfeld, H.T., Galin, T. and Hall, R., 2014 U-Pb Detrital Zircon Ages from Sarawak: Changes in Provenance Reflecting the Tectonic Evolution of Southeast Asia. In: American Geophysical Union, Fall Meeting 2014, abstract #V43D-4921.

Breitfeld, H.T., Hall, R., Galin, T., Forster,M.A. and BouDagher-Fadel, M.K., 2017 A Triassic to Cretaceous Sundaland–Pacific subduction margin in WestSarawak, Borneo. Tectonophysics 694, 35-56.

Burger, K., Zhou, Y. and Ren, Y., 2002 Petrography and geochemistry of tonsteins from the 4th Member of the Upper Triassic Xujiahe Formation in southern Sichuan Province, China. International Journal of Coal Geology 49, 1-17.

Carlile, J.C. and Mitchell, A.H.G., 1994 Magmatic arcs and associated gold and copper mineralization in Indonesia (special issue) In: van Leeuwen, T.M., Hedenquist, J.W., James, L.P., Dow, J.A.S. (Eds.), Journal of Geochemical Exploration 50, 91-142.

Christidis, G.E., 1998 Comparative study of the mobility of major and trace elements during alteration of an andesite and a rhyolite to bentonite, in the islands of Milos and Kimolos, Aedean, Greece. Clays and Clay Minerals 46, 379-399.

Christidis, G.E. and Huff, W.D., 2009 Geological aspects and genesis of bentonites. Elements 5, 93-98.

Clements, B., Burgess, P.M., Hall, R. and Cottam, M.A., 2011 Subsidence and uplift by slab-related mantle dynamics: a driving mechanism for the Late Cretaceous and Cenozoic evolution of continental SE Asia? Geological Society of London Special Publication 355, 37-51.

Clift, P., Lee, G.H., Nguyan, A.D., Barckhausen, U., Long, H. and Zhen, S., 2008 Seismic reflection evidence for a Dangerous Grounds miniplate: No extrusion origin for the South China Sea. Tectonics 27, 1-16.

Cochran, M.F. and Berner, R.A., 1996 Promotion of chemical weathering by higher plants: Field observations on Hawaiian basalts. Chemical Geology 132, 71-77.

Condie, K.C., 1993 Chemical composition and evolution of the upper continental crust: contrasting results from surface samples and shales. Chemical Geology 104, 1-37.

Corfu, F., Hanchar, J.M., Hoskin, P.W.O. and Kinny, P., 2003 Atlas of Zircon Textures. In: Zircon, Hanchar, J.M., Hoskin, P.W.O.,(Eds.). Reviews in Mineralogy and Geochemistry 53, Mineralogical Society of America and the Geochemical Society, 469-500.

Cottam, M., Hall, R., Sperber, C., Armstrong, R., 2010 Pulsed emplacement of layered granite: new high-precision age data from Mount Kinabalu, North Borneo. Journal of Geological Society of London 176, 49-60.

Cottam, M.A., Hall, R., Sperber, C. Kohn, B.P., Forster, M.A. and Batt, G.E., 2013 Neogene rock uplift and erosion in northern Borneo: evidence from the Kinabalu granite, Mount Kinabalu. Journal of the Geological Society, 170, 805-816.

Crow, M.J., 2005 Tertiary volcanicity. In: Barber, A.J., Crow, M.J., Milsom, J.S., (Eds.). Sumatra: Geology, Resources and Tectonic Evolution. Geological Society of London Memoir 31, 98-119.

Cullen, A., 2014 Nature and significance of the West Baram and Tinjar Lines, NW Borneo. Marine and Petroleum Geology 58, 674-686.

Cullen, A.B., Macpherson, C., Taib, N.I., Burton-Johnson, A., Geist, D., Spell, T. and Banda, R.A., 2013 Age and petrology of the Usun Apau and Linau Balui volcanics: windows to central Borneo's interior. Journal of Asian Earth Sciences 76, 372-388.

Davies, L., Hall, R. and Armstrong, R., 2014 Cretaceous crust in SW Borneo: petrological, geochemical and geochronological constraints from the Schwaner Mountains. Proceedings of Indonesian Petroleum Association, 38th Annual Convention and Exhibition,IPA14-G-025.

Demchuk, T. D. and Nelson-Glatiotis D. A., 1993 The identification and significance of kaolinite-rich, volcanic ash horizons (tonsteins) in the Ardley coal zone, Wabamun, Alberta, Canada. Bulletin of Canadian Petroleum Geology 41, 464-469.

de Silva, S., 1986 Stratigraphy of south Mukah-Balingian region, Sarawak. Newsletters of Geological Society of Malaysia 12, 215-219.

Dessert, C., Gaillardet, J., Dupre, G., Schott, Pokrovsky, O.S., 2009 Fluxes of high- versus low-temperature water–rock interactions in aerial volcanic areas: Example from the Kamchatka Peninsula, Russia. Geochimica et Cosmochimica Acta 73, 148-169.

Dix, G.R. and Al-Dulami, M.J., 2011 Late Ordovician (Chatfieldian) catastrophic volcanism and abrupt carbonate platform-interior subsidence: A tectonic link across a Taconian foreland basin (Québec Embayment) due to inherited crustal weakness. Geological Society of America Bulletin 123, 1988-2004.

Do Campo, M., del Papa, C., Jiménez-Millán, J. and Nieto, F., 2007 Clay mineral assemblages and analcime formation in a Palaeogene fluvial–lacustrine sequence (Maíz Gordo Formation Palaeogen) from northwestern Argentina. Sedimentary Geology 201, 56-74.

Do Campo, M., del Papa, C., Nieto, F., Hongn, F and Petrinovic, I., 2010 Integrated analysis for constraining palaeoclimatic and volcanic influences on clay–mineral assemblages in orogenic basins (Palaeogene Andean foreland, Northwestern Argentina) Sedimentary Geology 228, 98-112.

Donato, P., Albert, P.G., Crocitti, M., De Rosa, R. and Menzies, M.A., 2016 Tephra layers along the southern Tyrrhenian coast of Italy: Links to the X-5 & X-6 using volcanic glass geochemistry. Journal of Volcanology and Geothermal Research 317, 30-41.

Fauret, K., Willis, J.P. and Dreyer, J.C., 1996 The Grootegeluk Formation in the Waterberg Coalfield, South Africa: facies, palaeoenvironment and thermal history evidence from organic and clastic matter International Journal of Coal Geology 29, 147-186.

Feng, B.H., 1989 Permo-Carboniferous kaolinite from hydrolytic and altered volcanic ash sediments in north China. Acta Sedimitologica Sinica 7, 101-108.

Floyd, P.A., Leveridge, B.E., 1987 Tectonic environments of the Devonian Gramscatho basin, south Cornwall: framework mode and geochemical evidence from turbidites and sandstones. Journal of the Geological Society of London 144, 531–542.

Fontijn, K., Costa, F., Sutawidjaja, I., Newhall, C., and Herrin, J., 2015 A 5000-year record of multiple highly explosive mafic eruptions from Gunung Agung (Bali, Indonesia): implications for eruption frequency and volcanic hazards. Bulletin of Volcanology 77, 1-15.

Fuller, M., Ali, J.R., Moss, S.J., Frost, G.M., Richter, B. and Mahfi, A., 1999 Paleomagnetism of Borneo. Journal of Asian Earth Sciences 17, 3-24.

Galin, T., Breitfeld, H.T., Hall, R. and Sevastjanova, I., 2017 Provenance of the Cretaceous–Eocene Rajang Group submarine fan, Sarawak, Malaysia from light and heavy mineral assemblages and U-Pb zircon geochronology. Gondwana Research 51, 209-233.

Guo, Z.T, Sun, B., Zhang, S., Peng, S.Z., Xiao, G.Q., Ge, J.Y., Hao, Q.Z., Qiao, Y.S., Liang, M.Y., Liu, J.F., Yin, Q.Z. and Wei, J.J., 2008 A major reorganization of Asian climate by the early Miocene Climate of the Past 4, 153-174.

Grimes, C.B., Wooden, J.L., Cheadle, M.J. and John, B.E., 2015 "Fingerprinting" tectono-magmatic provenance using trace elements in igneous zircon. Contributions to Mineralogy and Petrology 170, 1-26.

Haile, N.S., 1974 Borneo. In: Spencer, A.M. (Ed.), Mesozoic-Cenozoic Orogenic belts: Data for Orogenic studies. Geological Society of London Special Publication 4, 333-347.

Hall, R., 2009 Southeast Asia's changing palaeogeography. Blumea 54, 148-161.

Hall, R., 2012 Late Jurassic–Cenozoic reconstructions of the Indonesian region and the Indian Ocean. Tectonophysics 570-571, 1-41.

Hall, R., 2013 Contraction and extension in northern Borneo driven by subduction Rollback. Journal of Asian Earth Sciences 76, 399-411.

Hall, R. and Sevastjanova, I., 2012 Australian crust in Indonesia. Australian Journal of Earth Sciences. 59, 827-844.

Hall, R. and Breitfeld, H.T., 2017 Nature and demise of the Proto-South China Sea. Bulletin of Geological Society of Malaysia 63 (in press).

Hall, R., van Hatttum, W.A. and Spakman, W., 2008 Impact of India–Asia collision on SE Asia: The record in Borneo. Tectonophysics 451, 366-389.

Hakimi, M. H., Abdullah, W. H., Sia, S-G. and Makeen, Y. M., 2013 Organic geochemical and petrographic characteristics of Tertiary coals in the northwest Sarawak, Malaysia: Implications for palaeoenvironmental conditions and hydrocarbon generation potential. Marine and Petroleum Geology 48, 31-46.

Hennig, J., Breitfeld, H.T., Hall, R. and Surya Nugraha, A.M., 2017 The Mesozoic tectono-magmatic evolution at the Paleo-Pacific subduction zone in West Borneo, Gondwana Research 48, 292-310.

Haq, B.U., Hardenbol, J. and Vail, P.R., 1987 Chronology of fluctuating sea levels since the Triassic. Science 235, 1156-1167.

Hay, W.W.,Soeding, E., DeConto, R.M. and Wold, C.N., 2002 The Late Cenozoic uplift – climate change paradox. International Journal of Earth Sciences 91, 746-774.

Hayashi, K., Fujisawa, H., Holland, H.D. and Ohmoto, H., 1997 Geochemistry of 1.9 Ga sedimentary rocks from northeastern Labrador, Canada. Geochimica et Cosmochimica Acta 61, 4115-4137.

He, B., Xu, Y., Zhong, Y. and Guan, J., 2010 The Guadalupian–Lopingian boundary mudstones at Chaotian (SW China) are clastic rocks rather than acidic tuffs: Implication for a temporal coincidence between the end-Guadalupian mass extinction and the Emeishan volcanism. Lithos 119, 10-19.

Hoskin, P.W.O., Ireland, T.R., 2000 Rare earth element chemistry of zircon and its use as a provenance indicator. Geology 28, 627-630.

http://volcano.si.edu/.

Hoskin, P.W.O. and Schaltegger, U., 2003 The composition of zircon and igneous and metamorphic petrogenesis. Reviews in Mineralogy and Geochemistry 53, 27-62.

Huang, H., Cawood, P.A., Hou, M., Yang, J., Ni, S., Du, Y. Yan, Z. and Wang, J., 2016 Silicic ash beds bracket Emeishan Large Igneous province to 1 m.y. at ~260 Ma. Lithos 264, 17-27.

Hutchison, C.S., 1996 The 'Rajang Accretionary Prism' and 'Lupar Line' problem of Borneo. In: Hall, R., Blundell, D.J. (Eds.). Tectonic Evolution of SE Asia. Geological Society of London Special Publication 106, 247-261.

Hutchison, C.S., 2005 Geology of North-west Borneo: Sarawak, Brunei and Sabah, I Edition, Elsevier, New York, USA. 421p.

Hutchison, C.S., Bergman, S.C., Swauger, D.A. and Graves, J.E., 2000 A Miocene collisional belt in North Borneo: uplift mechanism and isostatic adjustment quantified by thermochronology. Journal of the Geological Society of London 157, 783-793.

Keller, M. and Lehnert, O., 2010 Ordovician paleokarst and quartz sand: Evidence of volcanically triggered extreme climates? Palaeogeography, Palaeoclimatology, Palaeoecology 296, 297-309.

Kessler, F.L. and Jong, J., 2015 Incision of rivers in Pleistocene gravel and conglomeratic terraces:Further circumstantial evidence for the uplift of Borneo during the Neogene and Quaternary. Bulletin of the Geological Society of Malaysia 61, 49-57.

Kilian, R., Hohner, M., Biester, H., Wallrabe-Adams, H. J. and Stern, C. R., 2003 Holocene peat and lake sediment tephra record from the southernmost Chilean Andes (53–55°S), Reviews in Geology of Chile 30, 23–37.

Kiipli, T., Kiipli, E., Kallaste, T., Hints, R., Somelar, P. and Kirsimae, K., 2007 Altered volcanic ash as an indicator of marine environment, reflecting pH and sedimentation rate - example from the Ordovician Kinnekulle bed of Baltoscandia. Clays and Clay Minerals, 55, 177-188.

Kirk, H.J.C., 1957 The geology and mineral resources of the Upper Rajang and adjacentareas.British Territories Borneo Region Geological Survey Memoir 8, 181p.

Leech, M.L., Singh, S.,Klemperer, A.K., Jain, S.L. and Manickavasagam, R.M., 2005 The onset of IndiaAsia continental collision: Early, steep subduction required by the timing of UHP metamorphism in the western Himalaya. Earth and Planetary Sciences Letters 234, 83-97.

Liechti, P., Roe, RW. and Haile, N.S., 1960 The geology of Sarawak, Brunei and the western part of North Borneo. Geological Survey Department, British Territories in Borneo, Bulletin 3, Kuching.

Liao, Z., Hu, W., Cao, J., Wang, X., Yao, S., Wu, H. and Wan, Y., 2016 Heterogeneous volcanism across the Permian–Triassic Boundary in South China and implications for the Latest Permian Mass Extinction: New evidence from volcanic ash layers in the Lower Yangtze Region, Journal of Asian Earth Sciences 127,197-210.

Light, M.P.R., Bird, D.J., Posehn, G.A., Hudi, M.A.A., 1994 Complex transtensional structures and the hydrocarbon potential of the Greater Sarawak Basin, Sarawak as defined by synthetic aperture radar. Bulletin of Geological Society of Malaysia 36, 145-156.

Liu, X., Dong, B., Yin, Z., Smith, R.S. and Guo, Q., 2017 Continental drift and plateau uplift control origination and evolution of Asian and Australian monsoons. Scientific Reports 7, doi: 10.1038/srep40344.

Lowe, D.J. 2011 Tephrochronology and its application: a review. Quaternary Geochronology 6, 107-153.

Macpherson, CG., Chiang, K.K., Hall, R., Nowell, G.M.,Castillo, P.R. and Thirlwall, M.F., 2010 Plio-Pleistocene intra-plate magmatism from the southern Sulu Arc, Semporna peninsula, Sabah, Borneo: Implications for high-Nb basalt in subduction zones. Journal of Volcanology and Geothermal Research 190, 25-38.

Madon, M., 1999 Geological setting of Sarawak. In: The Petroleum Geology and Resources of Malaysia. PETRONAS, Kuala Lumpur, pp. 275-290.

Mathew, M. J., Menier, D., Siddiqui, N., Ramkumar, M., Santosh, M., Kumar, S., Hassan, M. 2016a Drainage basin and topographic analysis of a tropical landscape: Insights into surface and tectonic processes in northern Borneo. Journal of Asian Earth Sciences, 124, 14-27.

Mathew, M. J., Menier, D., Siddiqui, N., Kumar, S. G., Authemayou, C., 2016b Active tectonic deformation along rejuvenated faults in tropical Borneo: Inferences obtained from tectono-geomorphic evaluation. Geomorphology, 267, 1-15.

Mat-Zin, I.C., 1996 Tertiary tectonics and sedimentation history of the Sarawak basin, east Malaysia. Ph.D. Thesis, Durham University, 277p.

Mat-Zin, I.C., 2000 Stratigraphic Position of the Rangsi Conglomerate in Sarawak. Proceedings Annual Geological Conference 2000, Geological Society of Malaysia, pp.131-136.

Mat-Zin, I.C. and Tucker, M.E., 1999 An alternative stratigraphic scheme for the Sarawak Basin. Journal of Asian Earth Sciences 17, 215-232.

McLennan, S.M., 2001 Relationships between the trace element composition of sedimentary rocks and upper continentalcrust. Geochemistry, Geophysics, Geosystems 2, http://dx.doi.org/10.1029 /2000GC000109.

McLennan, S.M., Hemming, S., McDaniel, D.K. and Hanson, G.N., 1993 Geochemical approaches to sedimentation, provenance and tectonics. Geological Society ofAmerica Special Papers 284, 21-40.

Metcalfe, I., 2011 Tectonic framework and Phanerozoic evolution of Sundaland. Gondwana Research 19, 3-21.

Morley, R.J., 2010 Palaeoecology of Tropical Podocarps. In: Turner, B.L., Cernusak,L.M. (Eds.). Ecology of the Podocarpaceae in Tropical Forests. Smithsonian Institution Contributions to Botany, Smithsonian Institution Scholarly Press, Washington, DC.

Moss, S. J., 1998 Embaluh Group turbidites in Kalimantan: Evolution of a remnant oceanic basin in Borneo during the Late Cretaceous to Palaeogene. Journal of the Geological Society 155, 509-524.

Muller, J., 1972 Palynological evidence for change in geomorphology, climate andvegetation in the Mio-Pliocene of Malesia. In: Ashton, P.S., Ashton, H.M. (Eds.). The Quaternary Era in Malaysia. Geography Department, University of Hull, Miscellaneous Series 13, 6-34.

Nagarajan, R., Roy, P.D., Jonathan, M.P., Lozano, R., Kessler, F.L. and Prasanna, M.V., 2014 Geochemistry of Neogene sedimentary rocks from Borneo Basin, East Malaysia: Paleo-weathering, provenance and tectonic setting. Chemie der Erde 74, 139-146.

Nagarajan R., Roy, P.D., Kessler, F.L., Jong, J, Dayong, V. and Jonathan, M.P., 2017 An integrated study of geochemistry and mineralogy of the Upper Tukau Formation, Borneo Island (East Malaysia): Sediment provenance, depositional setting and tectonic implications. Journal of Asian Earth Sciences 143, 77-94.

Nugraheni, R.D., Chow ,W.S. Rahman, A.H.A., Nazor, S.N,M. and Abdullah, M.F., 2014 Tertiary coal-bearing heterolithic packages as low permeability reservoir rocks in the Balingian Sub-basin, Sarawak, Malaysia. Bulletin of the Geological Society of Malaysia 60, 85-93.

Pearce, J.M. and Peate, D.W., 1995 Tectonic implications of the composition of volcanic arc magmas. Annual Review of Earth and Planetary Sciences 23, 251-285.

Pearce, J.A., Harris, N.B.W., and Tindle, A.G., 1984 Trace element discrimination diagrams forthe tectonic interpretation of granitic rocks. Journal of Petrology 25, 956-983.

Perrier, V., Meidla, T., Tinn, O. and Ainsaar, L., 2012 Biotic response to explosive volcanism: Ostracod recovery after Ordovician ash-falls. Palaeogeography, Palaeoclimatology, Palaeoecology 365, 166-183.

Pinto, L, Hérail, G., Moine, B., Fontan, F., Charrier, R., Dupré, B., 2004 Using geochemistry to establish the igneous provenances of the Neogene continental sedimentary rocks in the Central Depression and Altiplano, Central Andes. Sedimentary Geology 166, 157-183.

Prouteau, G., Maury, R.C., Sajona, F.G., Pubellier, M., Cotten, J. and Bellon, H., 2001 Lemagmatisme post-collisionnel du Nord-Ouest de Bornéo, produit de la fusiond'un fragment de croûte océanique ancré dans le manteau supérieur.Bulletin dela Société Géologique de France 172, 319-332.

Praetorius, S., Mix, A., Jensen, B., Froese, D., Milne, G, Wolhowe, M., Addison, J. and Prahl, F., 2016 Interaction between climate, volcanism, and isostatic rebound in Southeast Alaska during the last deglaciation. Earth and Planetary Science Letters 452, 79-89.

Reuter, M., Piller, W.E. and Erhart, C., 2012 A Middle Miocene carbonate platform under silici-volcaniclastic sedimentation stress (Leitha Limestone, Styrian Basin, Austria) — Depositional environments, sedimentary evolution and palaeoecology. Palaeogeography, Palaeoclimatology, Palaeoecology 350-352, 198-211.

Roser, B.P. and Korsch, R.J., 1986 Determination of tectonic setting of sandstone-mudstone suites using SiO_2 content and K_2O/Na_2O ratio. Journal of Geology 94, 635-650.

Royer, D.L., 2006 CO_2-forced climate thresholds during the Phanerozoic. Geochimica et Cosmochimica Acta 70, 5665-5675.

Scudder, R.P., Murray, R.w., Schindlbeck, J.C., Kutterolf, S., Hauff, F., Underwoods, M.B., Gwizd, S., Lauzon, R. and McKinley, C.C., 2016 Geochemical approaches to the quantification of dispersed volcanic ash in marine sediment. Progress in Earth and Planetary Science 3:1, DOI 10.1186/s40645-015-0077-y.

Shen, J., Algeo, T.J., Hu, Q., Zhang, N., Zhou, L., Xia, W., Xie, S. and Feng, Q., 2012 Negative C-isotope excursions at the Permian-Triassic boundary linked to volcanism. Geology 40, 963-966.

Shen, J., Algeo, T.J., Hu, Q., Xu, G., Zhou, L. and Feng, Q., 2013 Volcanism in South China during the Late Permian and its relationship to marine ecosystem and environmental changes. Global and Planetary Change 105, 121-134.

Shuib, M.K., 2003 A dextral strike-slip model for the Miri Structure. Geological Society of Malaysia Bulletin 47, 95-103.

Sia, S.G., Wan Hasiah, A., Konjing, Z. and Koraini, A.M., 2014 The age, palaeoclimate, palaeovegetation, coal seam architecture/mire types, paleodepositional environments and thermal maturity of syn-collision paralic coal from Mukah, Sarawak, Malaysia. Journal of Asian Earth Sciences 81, 1-19.

Sia, S.G. and Wan Hasiah, A., 2011 Concentration and association of minor and trace elements in Mukah coal from Sarawak, Malaysia, with emphasis on the potentially hazardous trace elements. International Journal of Coal Geology 88, 179-193.

Soeria-Atmadja, R., Noeradi, D. and Priadi, B., 1999 Cenozoic magmatism in Kalimantan and its related geodynamic evolution. Journal of Asian Earth Sciences 17, 25-45.

Sowerbutts, A., 2000 Sedimentation and volcanism linked to multiphase rifting in an Oligo-Miocene intra-arc basin, Anglona, Sardinia. Geological Magazine 137, 395-418.

Spalletti, L.A., Queralt, I., Matheos, S.D., Colombo, F. and Maggi, J., 2008 Sedimentary petrology and geochemistry of siliciclastic rocks from the upper Jurassic Tordillo Formation (Neuque´n Basin, western Argentina): Implications for provenance and tectonic setting. Journal of South American Earth Sciences 25, 440-463.

Stollhofen, H., Stanistreet, I.G., Bangert, B. and Grill, B., 2000 Tuffs, tectonism and glacially related sea-level changes, Carboniferous–Permian, southern Namibia. Palaeogeography, Palaeoclimatology, Palaeoecology 161, 127-150.

Sun, S.S., McDonough, W.F., 1989 Chemical and isotopic systematics of oceanic basalts: implications for mantle composition and processes. In: Saunders, A.D., Norry, M.J. (Eds.), Magmatism in Ocean Basins. Geological Society of London Special Publication, pp. 313-345.

Tan, D.N.K., 1979 Lupar Valley, West Sarawak, Malaysia. Geological Survey of Malaysia Reports 13, 39-49.

Tan, D.N.K., 1993 Geology of the Kuching area, West Sarawak, Malaysia. Geological Suvey of Malaysia Report. 19p.

Tate, R.B., 1991 Cross-border correlation of geological formations in Sarawak and Kalimantan. Bulletin of Geological Society of Malaysia 28, 63-96.

Tomlinson, E.L., Smith, V.C., Albert, PG., Aydar, E., Civetta, L., Cioni, R, Cubukcu, E., Gertisser, R., Isaia, R., Menzies, M.A., Orsi, G., Rosi, M. and Zanchetta, G., 2015 The major and trace element glass compositions of the productive Mediterranean volcanic sources: tools for correlating distal tephra layers in and around Europe. Quaternary Science Reviews 118, 48-66.

van Gorsel, J.T., 2012 Bibliography of the geology of Indonesia and surrounding areas, 4.1 Edition. www.vangorselslist.com.

van Hattum, M.W.A., 2005 Provenance of Cenozoic sedimentary rocks of northern Borneo. Ph.D. Thesis, University of London, 457 pp.

van Hattum, M.W.A., Hall, R., Pickard, A.L. and Nichols, G.J., 2006 SE Asian sediments not from Asia: Provenance and geochronology of North Borneo sandstones. Geology 34, 589-592.

van Hattum, M.W.A., Hall, R., Pickard, A.L. and Nichols, G.J., 2013 Provenance and geochronology of Cenozoic sandstones of northern Borneo. Journalof Asian Earth Sciences. 76, 266-282.

Verma, S.P. and Armstrong-Altrin, J.S., 2013 New multi-dimensional diagrams for tectonic discrimination of siliciclastics sediments and their application to Precambrian basins. Chemical Geology 355, 117-133.

Wan Hasiah, A., 2003 Coaly source rocks of NW Borneo: role of suberinite and bituminite in oil generation and expulsion. Bulletin Geological Society Malaysia 47, 153-163.

Wang, W., Zheng, W., Zhang, P., Li, Q., Kirby, E., Yuan, D., Zheng, D., Liu, C.,Wang, Z., Zhang, H. andPang, J., 2017 Expansion of the Tibetan Plateau during the Neogene. Nature Communications 8, doi: 10.1038/ncomms15887.

Ward, P.L., 2009 Sulfur dioxide initiates global climate change in four ways. Thin Solid Films 517, 3188-3203.

Williams, P., Supriatna, S., Harahap, B., 1986 Cretaceous mélange in West Kalimantan and its tectonic implications. Bull. Geol. Soc. Malaysia 19, 69-78.

Williams, P.R. and Harahap, B.H., 1987 Preliminary geochemicaland age data from post-subduction intrusive rocks, northwest Borneo. Australian Journal of Earth Sciences 34, 405-415.

Williams, P. R., Johnston, C.R., Almond, R. A. and Simamora, W.H., 1988 Late Cretaceous to Early Tertiary structural elements of West Kalimantan. Tectonophysics 148, 279-297.

WIllIamson, I.T. and Bell, B.R., 2012 The Staffa Lava Formation: graben-related volcanism, associated sedimentation and landscape character during the early development of the Palaeogene Mull Lava Field, NW Scotland. Scottish Journal of Geology 48, 1-46.

Wolfendren, E.B., 1960 The geology and mineral resources of the Lower Rajang Valley and adjoining areas, Sarawak. Geological Survey of British Borneo Memoir 11, 167 p.

Yuan, H.L., Gao, S., Liu, X.M., Li, H.M., Gunther, D., Wu, F.Y., 2004 Accurate U-Pb age and trace element determination of zircon by laser ablation-inductively coupled plasma-mass spectrometry. Geostandards and Geoanalytical Research 28, 353-370.

FIGURE AND TABLE CAPTIONS

Fig. 1. Regional geology and location of the study area. The Borneo region was subjected to multiple episodes of tectono-magmatic events. **A:** shows the regional topography, geology and magmatic events (Volcanism data gathered from the Global Volcanism Program, Smithsonian Institution; http://volcano.si.edu/ and Hall, 2009). Inset square shows the location of the study area. **B:** Geology of the study area (modified after Hakimi et al., 2013). The figure also shows the outcrops and sampled locations.

Fig. 2. Regional stratigraphic framework (after Mat-Zin, 2000; Hutchison, 2005). Hall and Breitfeld (2017) termed the major unconformity as Rajang Unconformity and assigned a slightly different age. Few recent studies including, Hall and Sevastjanova (2012), Hall et al., (2008) and Hall (2012) have questioned the Sarawak Orogeny and have interpreted it as a regional change in plate boundaries rather than a collision event. Nevertheless, we used this stratigraphic setup, only *per se*, rather than our attestation to the orogeny, terminology etc., as our study was not exactly at the same scale of tectonic and other processes discussed in these papers.

Fig. 3. Occurrence of ash layer interbedded between thick coal seams. Figure 3A depicts the excellent preservation of tephra layer inter-bedded between very thick sub-bituminous coal deposits, as exposed in a quarry section. The coal seams are sandwiched between coastal plain sandstones. The overlying very thick, massive sandstone shows the occurrences of inter-bedded feebly cross-bedded, coarse sandstones probably of shallow, ephemeral channel. The lithological association suggested prevalent vast coastal plains in which many lacustrine - swamp -ephemeral shallow fluvial channel depositional settings occurred. These depositional and facies associations (litholog in Fig. 3A) are akin to the present day coastal plains in which thick peat bogs develop and are periodically submerged/overlain by floods and flood deposits during extreme weather conditions. Similar conditions for the lithofacies association are interpreted. **Fig. 3B and Fig. 3C** show the close-up view of the ash layer sampled in the quarry section. **Fig. 3B** depicts the macroscopic view of a core sample recovered from the region, which was located about 5 km away from the quarry section shown in Fig. 3A. See Fig. 1B for the geographic distribution of the sampling sites and core recovery. The absence of any internal sedimentary structure, monotonously uniform color, texture, and contact relationships of the tephra layer can be observed from these photographs. The occurrence of sharp contact between the underlying coal seam and tephra layer (**Fig. 3E** shows few of the glass shards recovered from the quarry section and core samples) suggests a major erosional boundary, enforced by flooding of low-energy swamps during and/or immediately after the volcanic event. The resumption of swamp development after the flood receded and atmospheric fall-out ceased, is evidenced by the occurrence of a very thick coal seam over the tephra layer. The occurrence of poorly sorted, coarse-medium sandstone deposits with mottled /nodular texture at various stratigraphic levels and sporadically sandwiched channel deposits are evidence of the coastal plain development over a swamp-lacustrine depositional setting, perhaps due to excessive sediment influx, that cannot be transported offshore. The development of sandwiched shallow-ephemeral channels and rocks with mottled texture are evidence of a seasonal flood flow and episodic paleosol development. Please note the non-depositional contact between cycle IV and cycle V offshore, and absence of any stratigraphic record for the period between 13-11.5 Ma (Mat-Zin and Tucker, 1999). This information, together with the radiometric dating results of the present study implies a sea level rise and the cessation of offshore bypassing of terrestrial sediments as a result of or during the aftermath of the catastrophic volcanic event. As discussed in the following sections, this volcanic event was also associated with the magmatic Mt. Kinabalu pluton, in which case, the tephra layer straddles the boundary between tectonic quiescence (as revealed by formation of regoliths at basement and thick

coal seams) and active tectonics and exhumation of the basement (as revealed by lithofacies succession and rapidly changed depositional settings). This event explains major changes in climate, tectono-magmatic and depositional-erosional events of the region.

Fig. 4. Photomicrographs of volcanic glass shards found in the ash samples. Note the angular, transparent, non-crystalline nature as visible under plane polarized light. Highly varied size ranges could also be observed from the scale bars placed adjacent to individual grains. These characteristics support the inferences of volcanic origin, wind-blown nature, and atmospheric fallout of ejecta directly into the depositional site.

Fig. 5. X-ray diffractograms of the volcanic ash samples. The ubiquitous presence of kaolin, followed by quartz is indicated by X-Ray diffractograms. The abundance of kaolin indicates climatic conditions conducive for deep weathering of basement rocks followed by extensive exhumation coeval with volcanic activity (tectono-magmatic event?), occurrences of subordinate amounts of quartz and unidentified mineral species adjacent to the quartz peak in the XRD-chart, is presumably suggestive of silicic lava as the source and sediment recycling.

Fig. 6. Representative Cathodoluminescence (CL) images of zircon grains from volcanic ash samples (LFM-V.ASH-A, LFM-V.ASH-B, LFM-V.ASH-C). The ^{206}Pb/^{238}U ages in Ma are shown and the red circles indicate spots of LA-ICP-MS U-Pb dating. Despite variations in size and crystallographic characteristics, preservation of external morphology of zircon grains suggests their resistance to physical changes. The internal morphologies and U-Pb data of these grains suggest they were sourced from juvenile as well as older magmas, as well as recycling of basement rock sources, producing a mixture of polygenetic zircons in the tephra layer.

Fig. 7. Multi element diagram for average major and trace element concentrations of the volcanic ashes. Quarry section (n = 4) and core (n = 1) Mt. Pinatubo tephra (n = 1; reference) normalized against UCC (McLennan, 2001).

Fig. 8. REE of zircon grains. The data are normalized against chondrite values (Sun and McDonough, 1989) for their utility in determining magmatic provenance.

Fig. 9. U-Pb concordia plots (a, c, e), and ^{206}Pb/^{238}U mean age and age data histograms with probability curves (b, d, f) for the various zircon populations

Fig. 10. Bimodality of the sediment grains in ash layer. Note the typical dual size class that might have emanated from two different provenances/source areas/transport media.

Fig. 11. Source rock discriminant plots. A) Th/Sc versus Sc bivariate plot for volcanic ash samples. PAAS and UCC values are from Taylor and McLennan, 1985; McLennan, 2001, and granite, andesite, and basalt values are from Condie, 1993. **B) La/Th versus Hf bivariate diagram for the volcanic ash samples** (after Floyd and Leveridge, 1987).

Fig. 12. Cross plots of zircon trace element chemistry.

Fig. 13. Discrimination of tectonic setting (after Roser and Korsch, 1986; Verma and Armstrong-Altrin, 2013) **A)** Discriminant-function multi-dimensional diagram for high-silicaclastic sediments (Verma and Armstrong-Altrin 2013). The subscript m1 in DF1 and DF2 represents the high-silica diagram based on $\log_e$-ratios of major elements. The discriminant-function equations are the following:DF1(Arc-Rift-Col)m1=(−0.263×In(TiO$_2$/SiO$_2$)adj)+(0.604×In(Al$_2$O$_3$/SiO$_2$)adj)+(−1.725×In(Fe$_2$O$_3$t/SiO$_2$)adj)+(0.660×In(MnO/SiO$_2$)adj)+(2.191×In(MgO/SiO$_2$)adj)+(0.144×In(CaO/SiO$_2$)adj)+(−1.304×In(Na$_2$O/SiO$_2$)adj)+(0.054×In(K2O/SiO2)adj)+(−0.330×In(P$_2$O$_5$/SiO$_2$)adj)+1.588DF2(Arc-Rift Col)m1=(−1.196×In(TiO$_2$/SiO$_2$)adj)+ (1.604×In(Al$_2$O$_3$/SiO$_2$)adj)+(0.303×In(Fe$_2$O$_3$t/SiO$_2$)adj)+(0.436×In(MnO/SiO$_2$)adj)+(0.838×In(MgO/SiO$_2$)adj)+(−0.407×In(CaO/SiO$_2$)adj)+(1.021×In(Na$_2$O/SiO$_2$)adj)+(−1.706×In(K$_2$O/SiO$_2$)adj)+(−0.126×In(P$_2$O$_5$/SiO$_2$)adj)−1.068; **B)** Discriminant-function multi-dimensional diagram for low-silica clastic sediments (Verma and Armstrong-Altrin, 2013). The subscript m2 in DF1 and DF2 represents the low-silica diagram based on $\log_e$-ratio of major elements. Discriminant function equations are: DF1(Arc-Rift-Col)m2 =(0.608 ×In(TiO$_2$/SiO$_2$)adj) +(−1.854 _

ln(Al$_2$O$_3$/SiO$_2$)adj) +(0.299 ×ln(Fe$_2$O$_3$t/SiO$_2$)adj) +(−0.550 ×ln(MnO/SiO$_2$)adj) +(0.120 ×ln(MgO/SiO$_2$)adj) +(0.194 ×ln(CaO/SiO$_2$)adj) +(−1.510 ×ln(Na$_2$O/SiO$_2$)adj) +(1.941 ×ln(K$_2$O/SiO$_2$)adj) +(0.003 ×ln(P$_2$O$_5$/SiO$_2$) adj) −0.294 DF2(Arc-Rift-Col)m2 =(−0.554 ×ln(TiO$_2$/SiO$_2$)adj) +(−0.995 ×ln (Al$_2$O$_3$/SiO$_2$)adj) +(1.765 ×ln(Fe$_2$O$_3$t/SiO$_2$)adj) +(−1.391 ×ln(MnO/SiO$_2$)adj) +(−1.034 ×ln(MgO/SiO$_2$)adj) +(0.225 ×ln(CaO/SiO$_2$)adj) +(0.713 ×ln(Na$_2$O/SiO$_2$)adj) +(0.330 ×ln(K$_2$O/SiO$_2$)adj) +(0.637 ×ln(P$_2$O$_5$/SiO$_2$)adj) −3.631. **C)** SiO$_2$ vs. K$_2$O/Na$_2$O plot shows the tectonic setting discrimination fields for volcanic ash samples (after Roser and Korsch, 1986). **D)** U/Yb vs. Y (Grimes et al. 2007), distinguishing the possible tectonic setting of the volcanism that produced the zircon. **E)** Y vs. Nb and **F)** Yb vs.Ta discrimination diagrams of tectonic setting (after Pearce et al., 1984).

Fig. 14. Depositional setting, sediment sources and depositional model. A: Idealistic model depicting the regional topographic and depositional setting. Development of thick regolith, luxuriant vegetation, coastal plain-lacustrine-flood plain-swamps, probably supported by relatively favorable climate, tectonic quiescence prior to volcanic explosion are represented in this figure. **B:** Represents the inset "B" shown in "A". This figure depicts the distal volcanic event, associated atmospheric transport of ejecta to the coastal plains and swamps. **C:** Represents the inset "B" shown in "A". This figure depicts the atmospheric fallout of ejecta, sediment influx from older basement-regolith and their deposition into the swamps-organic matter bed. **D:** Represents the inset "B" shown in "A". Depiction of resumption of organic matter accumulation after the settling and influx of ejecta, followed much latter by enhanced siliciclastic influx that covered the coastal plains, swamps and lacustrine settings.

Fig. 15. Distribution of Miocene volcanic rock outcrops.

Table 1. Carbon content and loss on ignition of the studied ash and coal samples.
Table 2. Major oxides (wt %), trace and rare earth elements (ppm) data of the volcanic ashes from quarry, core and reference samples.
Table 3. Trace and REE of the zircon grains.
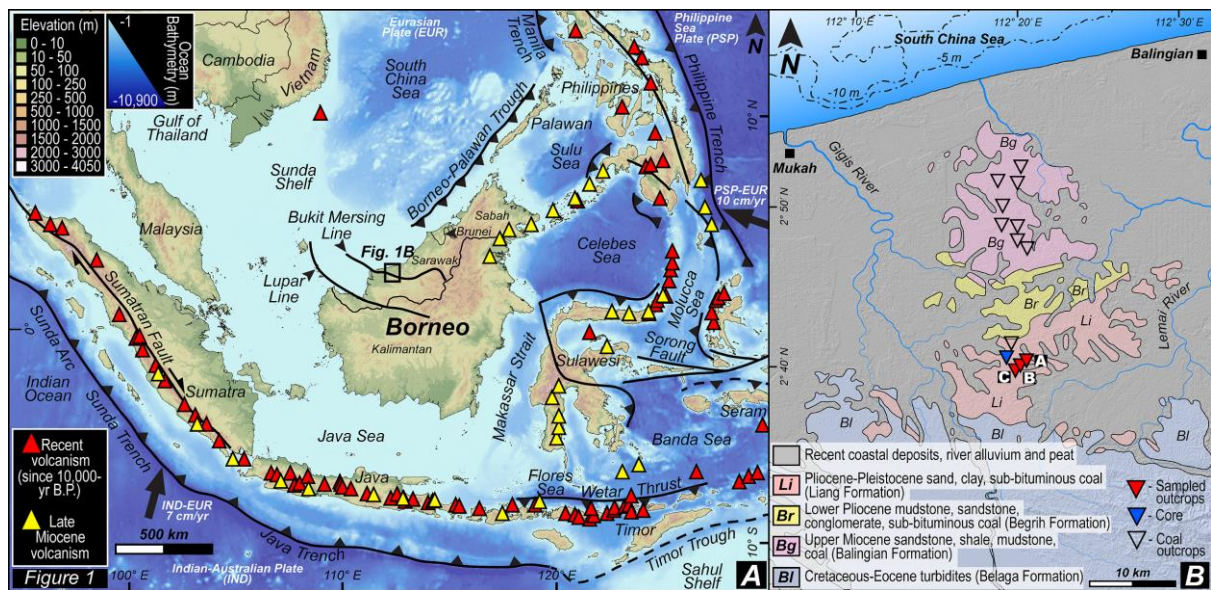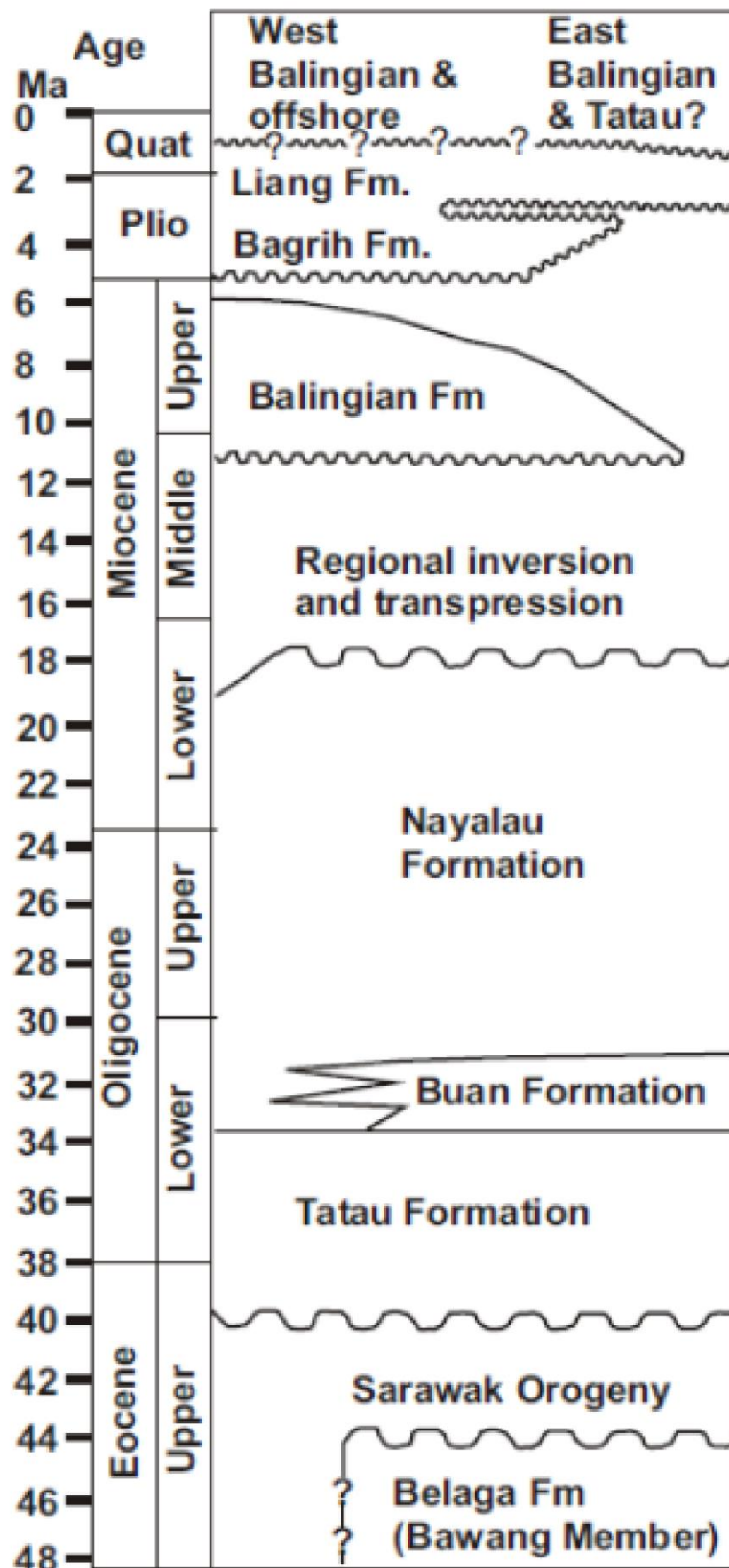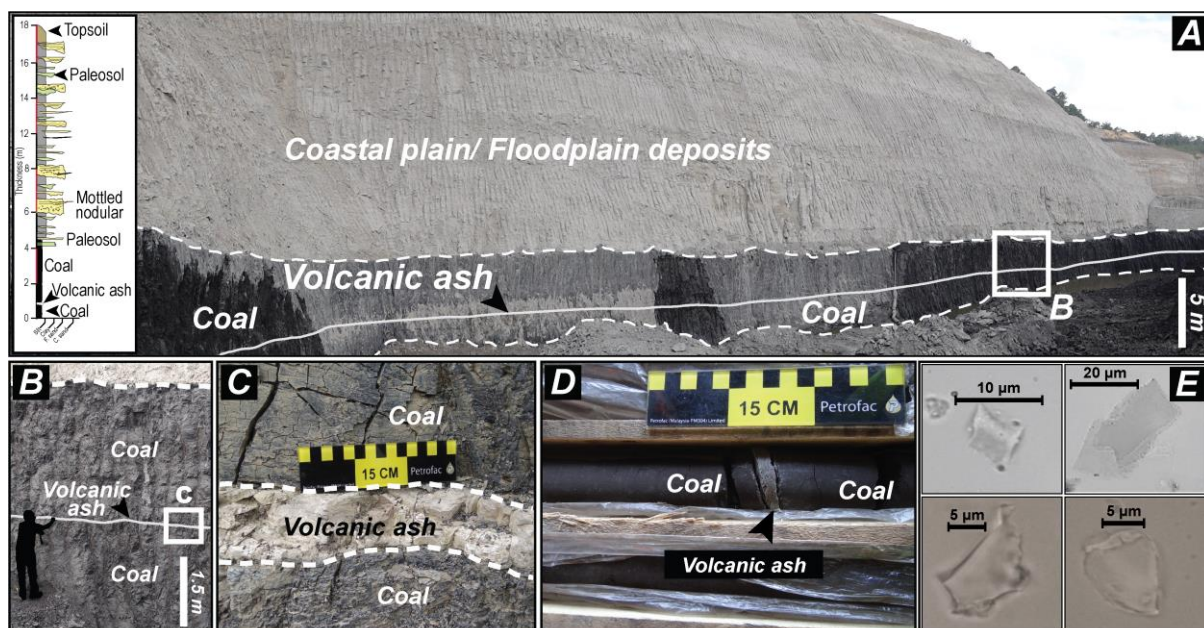
Figure 1

Figure 2
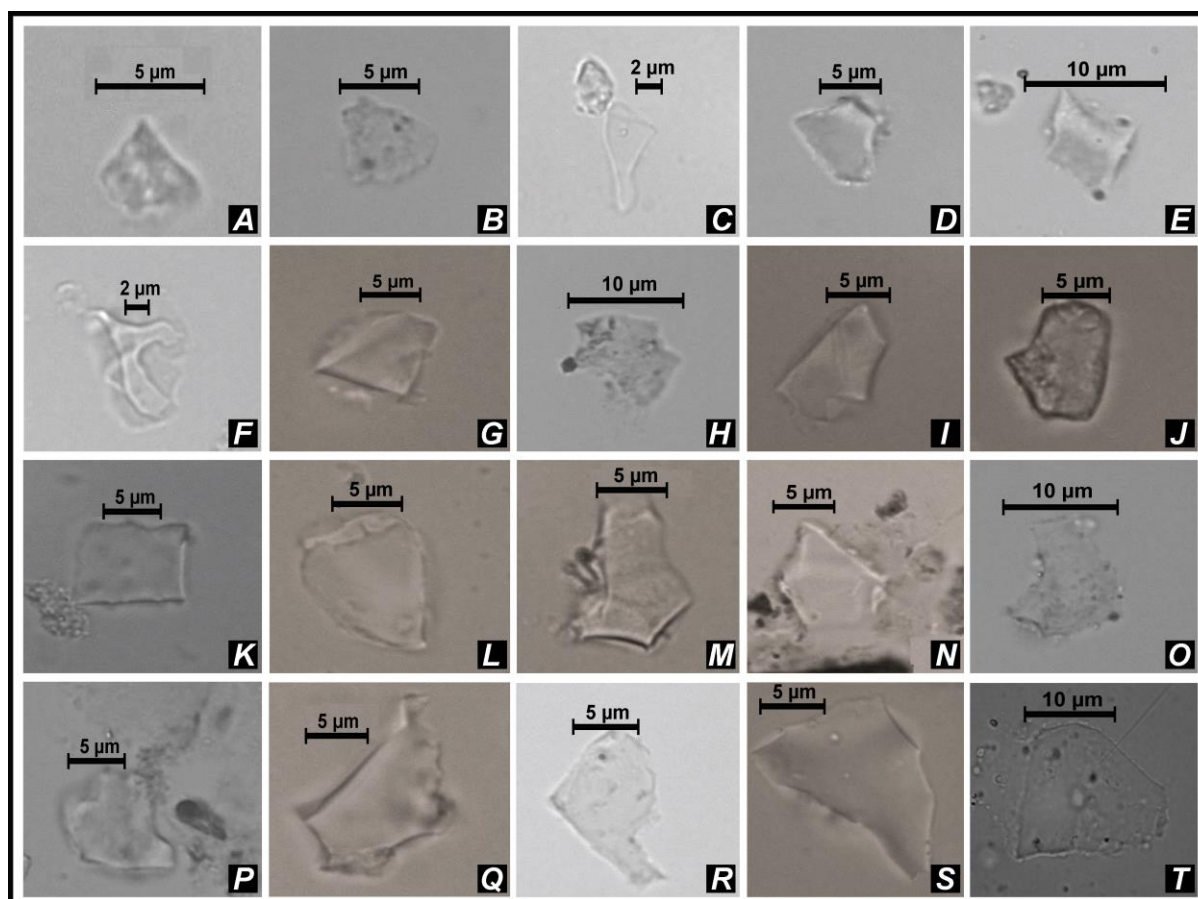
Figure 3

Figure 4
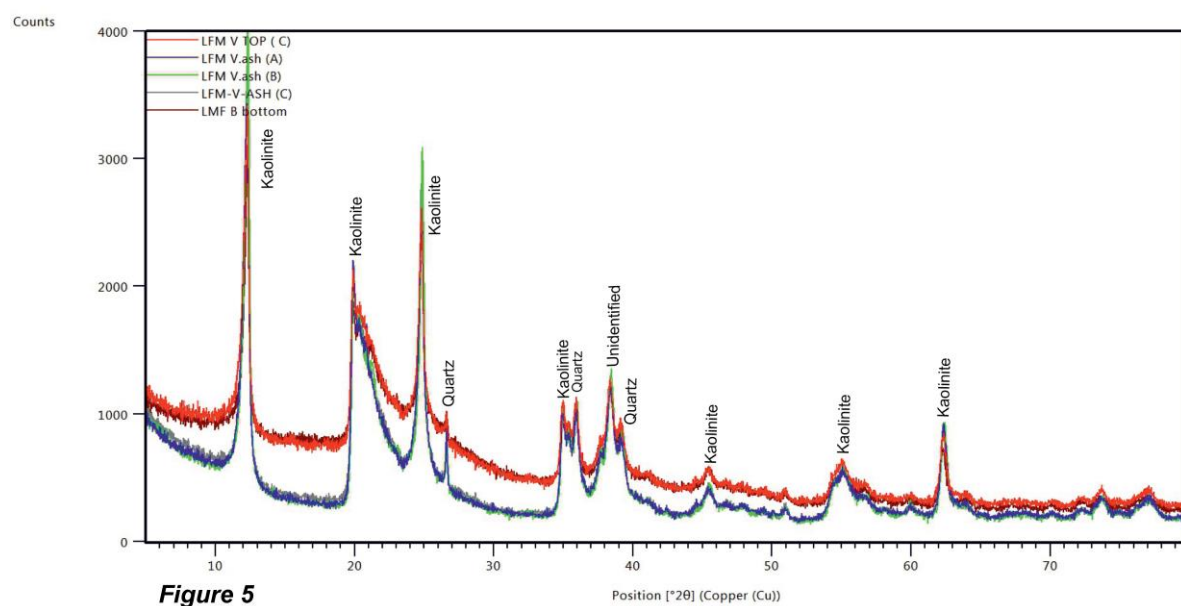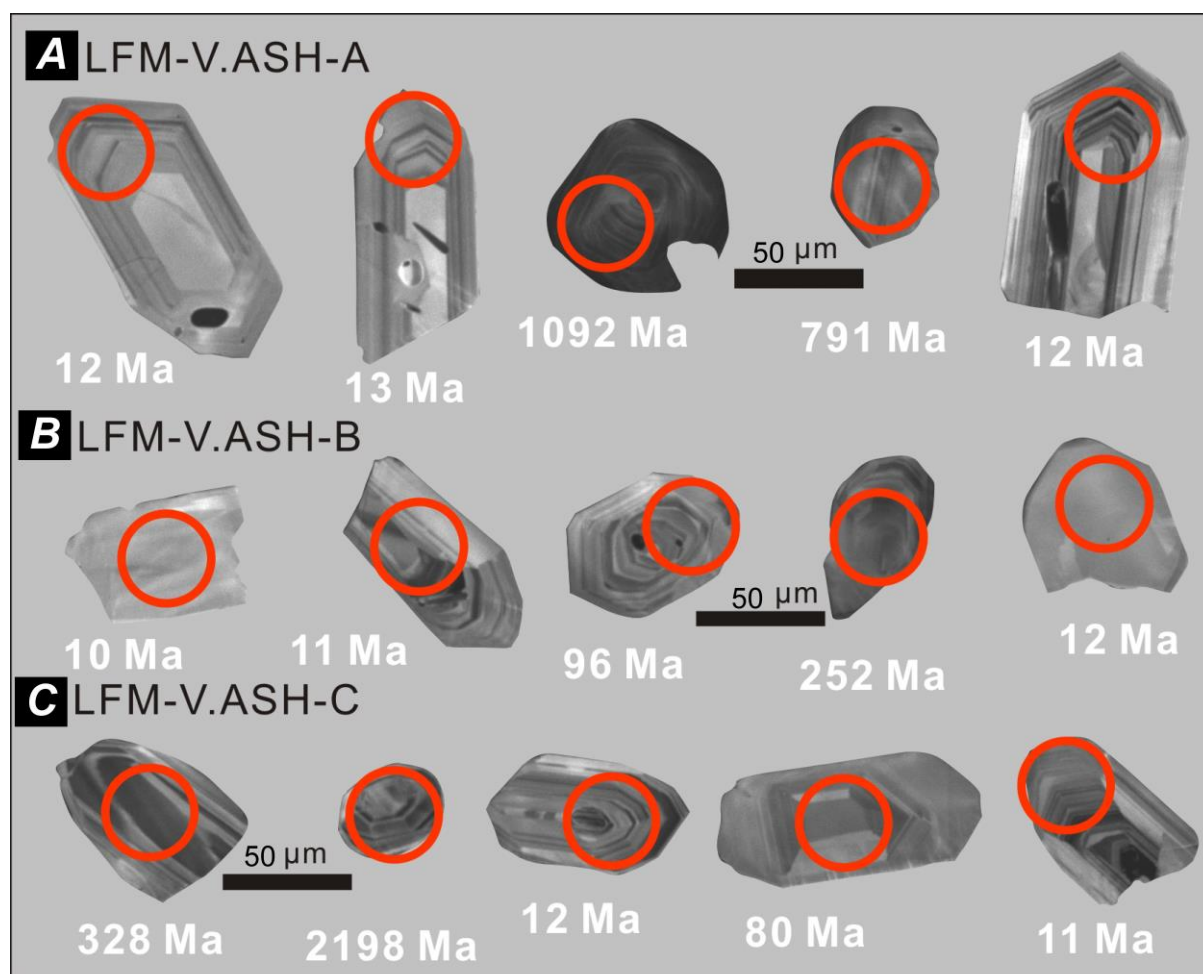
Figure 5

Figure 6

Figure 7

Figure 8

Figure 9A and 9B

Figure 9C and 9D

Figure 9E and 9F

Figure 10

Particle diameter (φ)

Figure 11

Figure 12

Figure 13A and 13B

Figure 13C and 13D
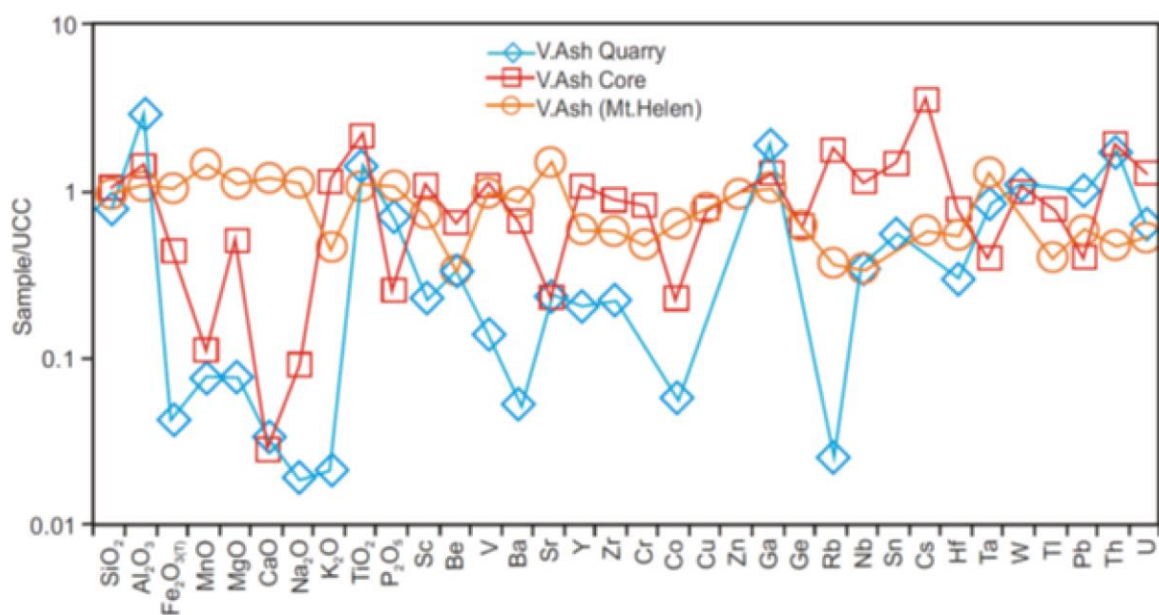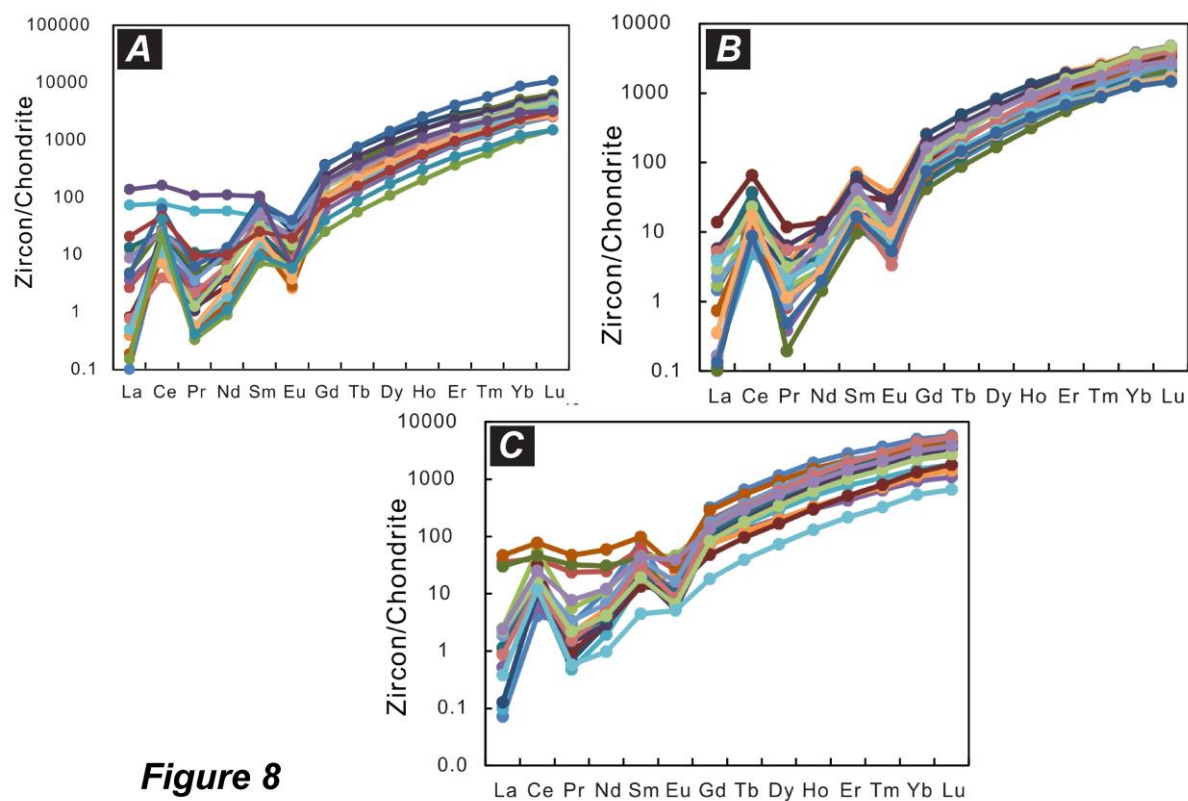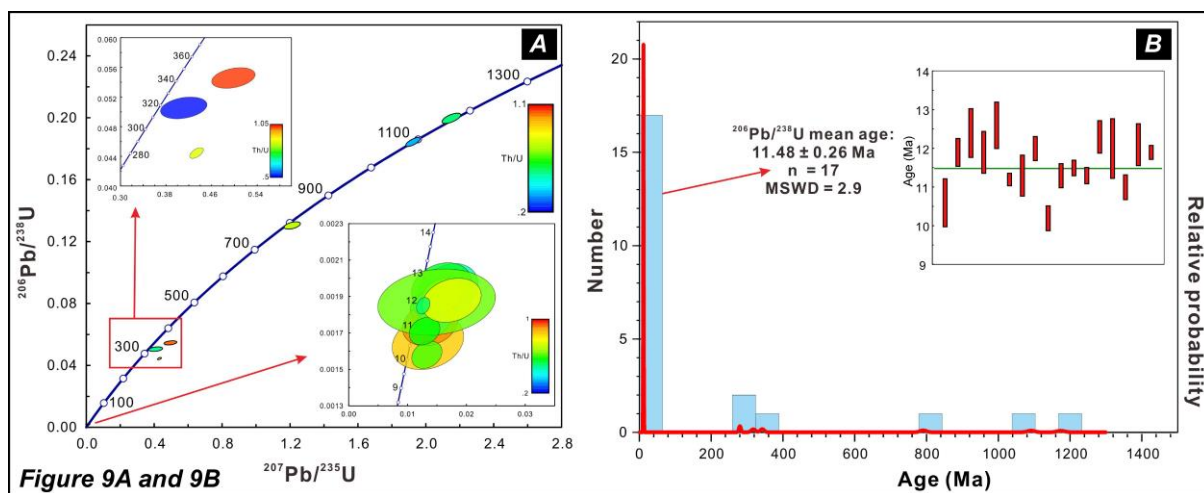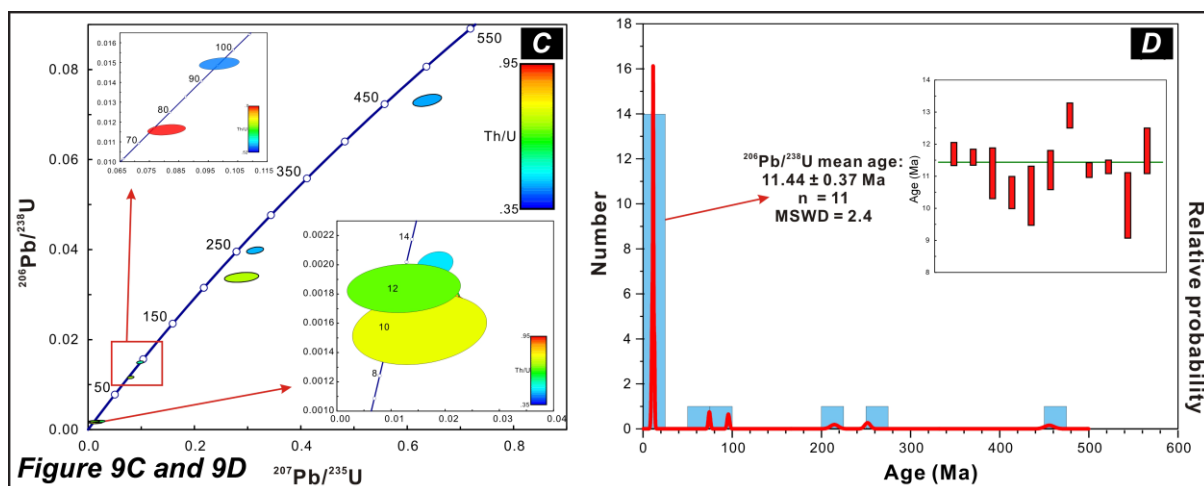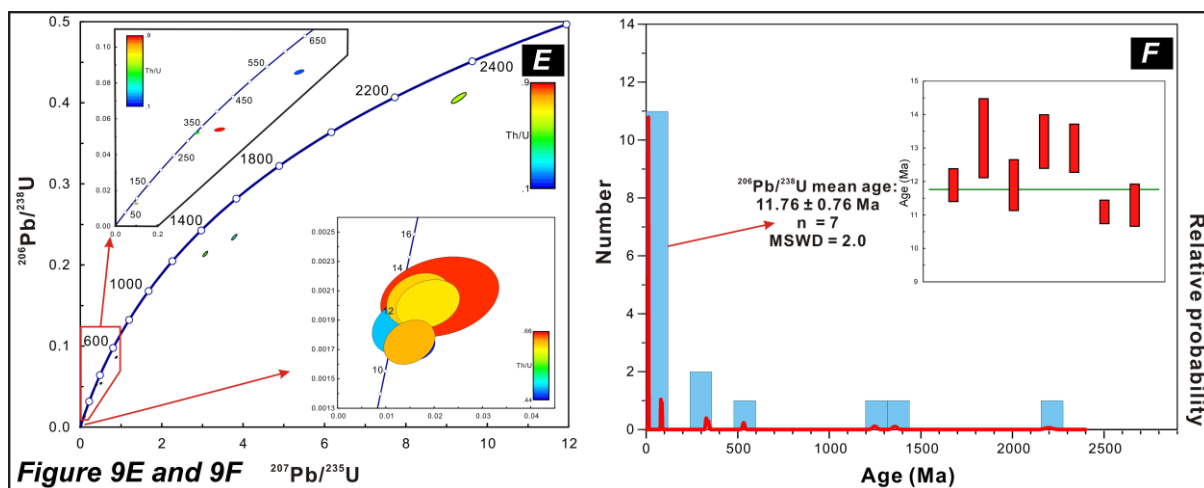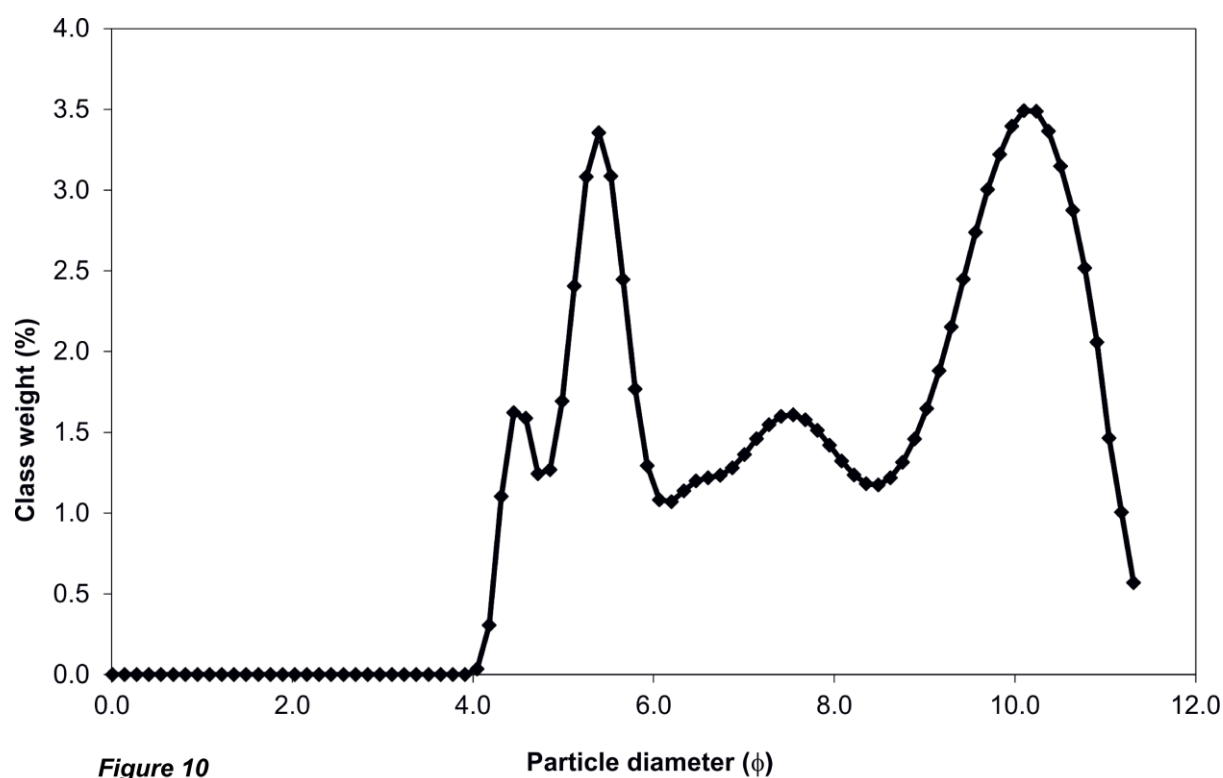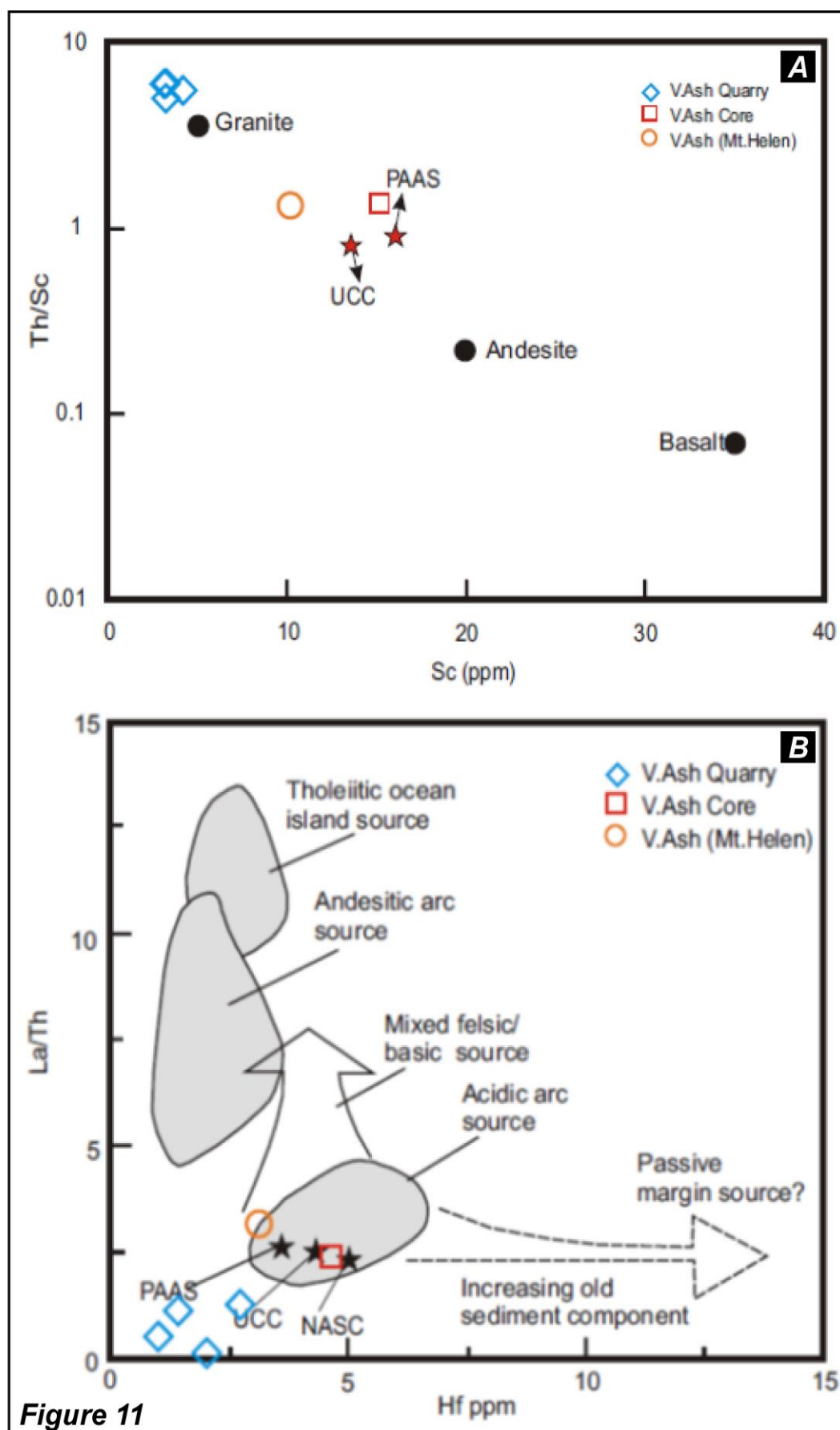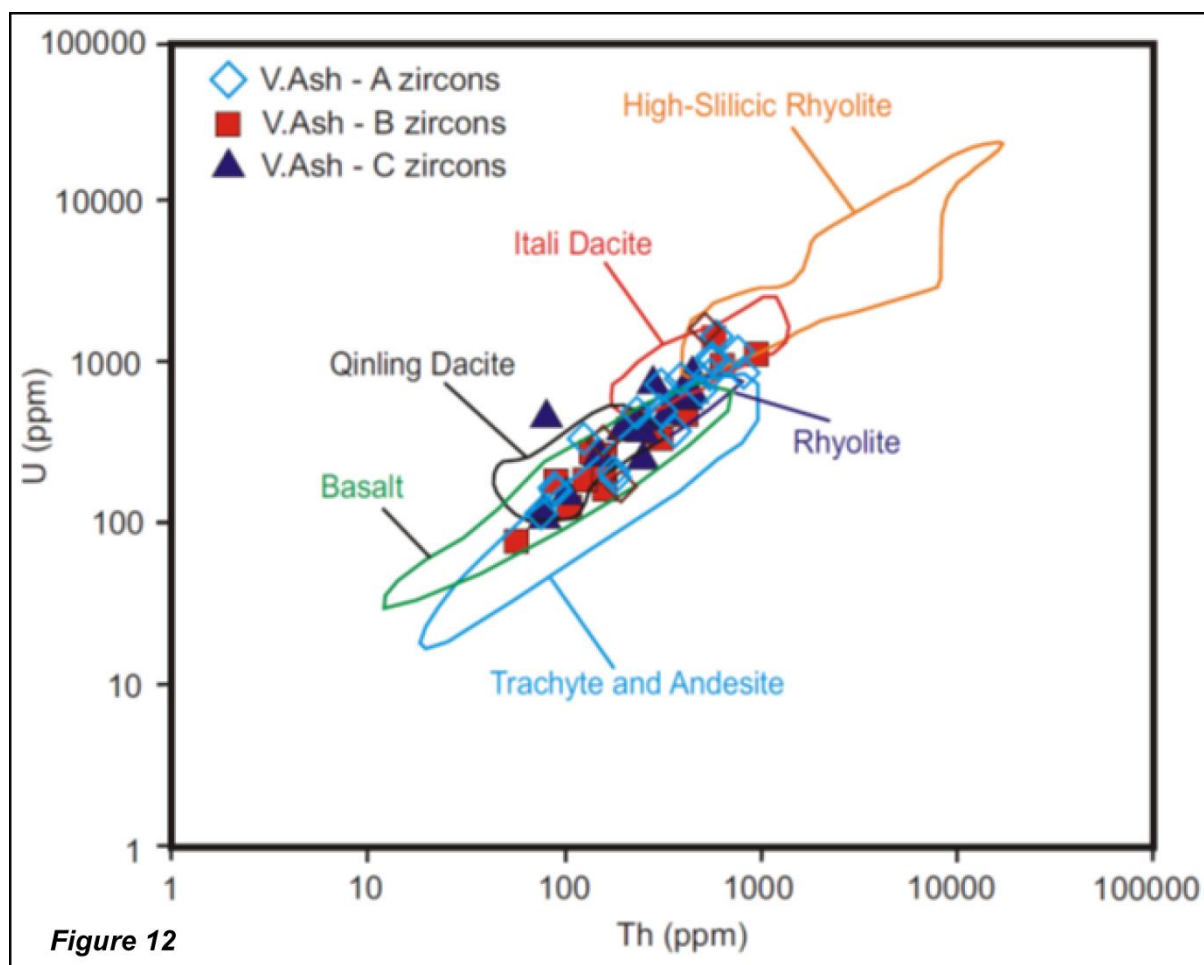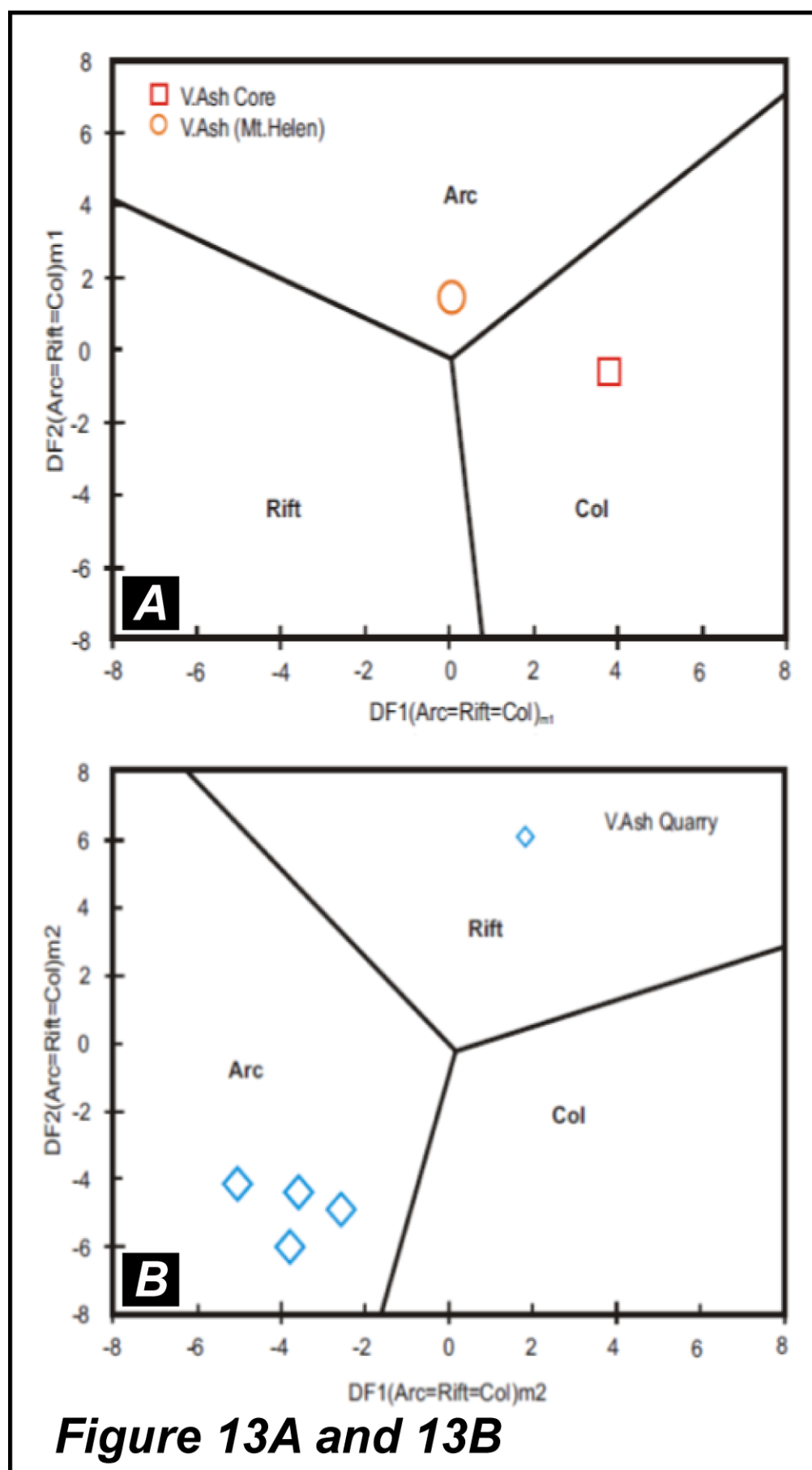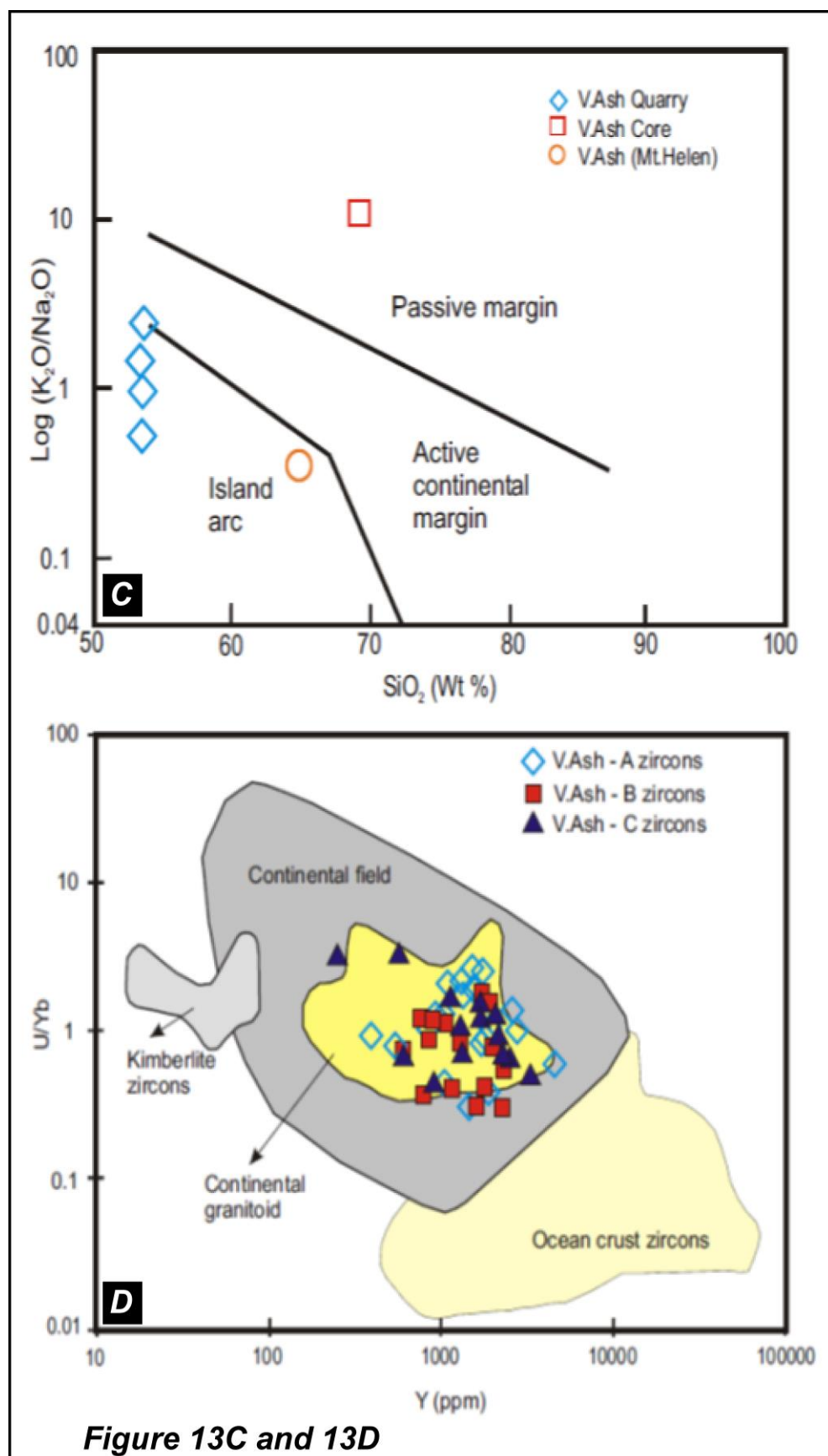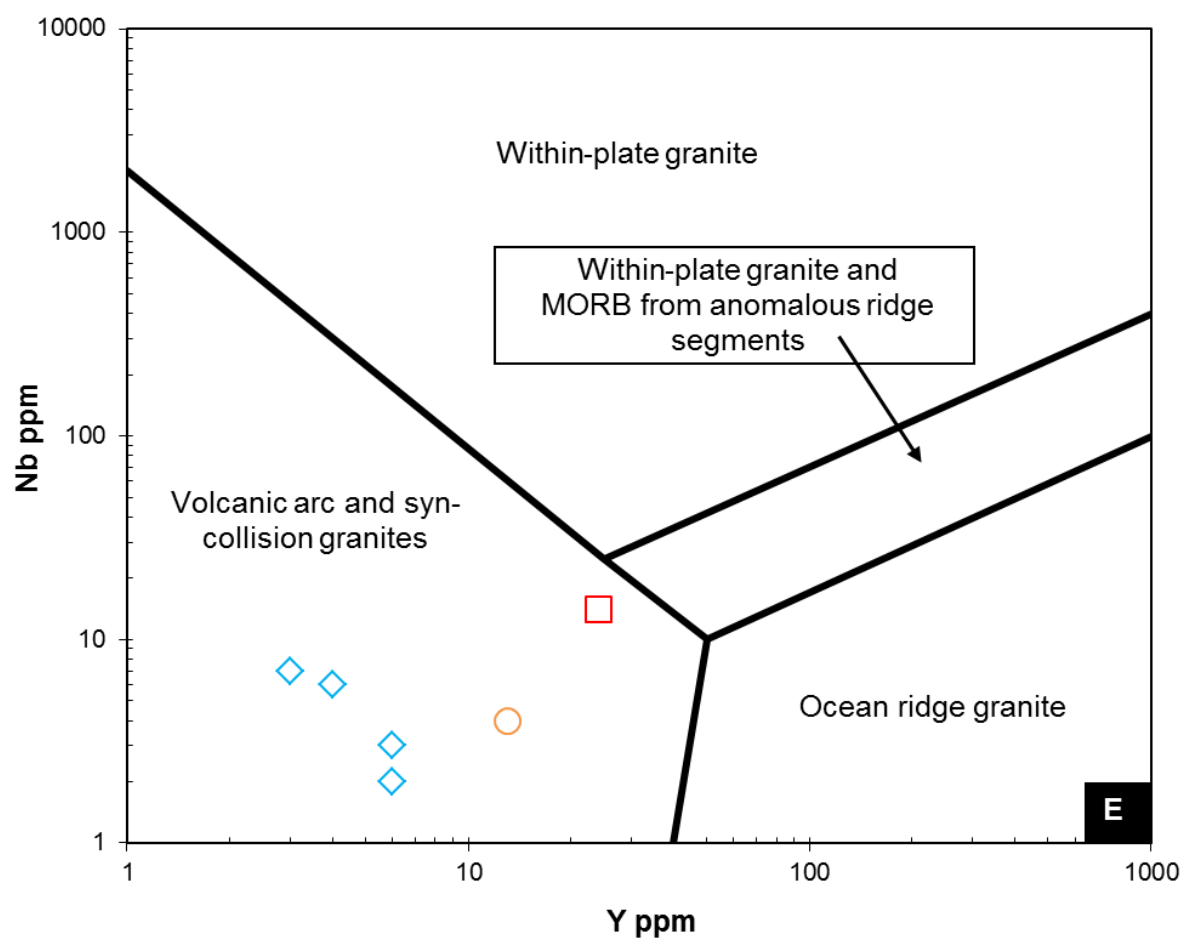
Figure 13E
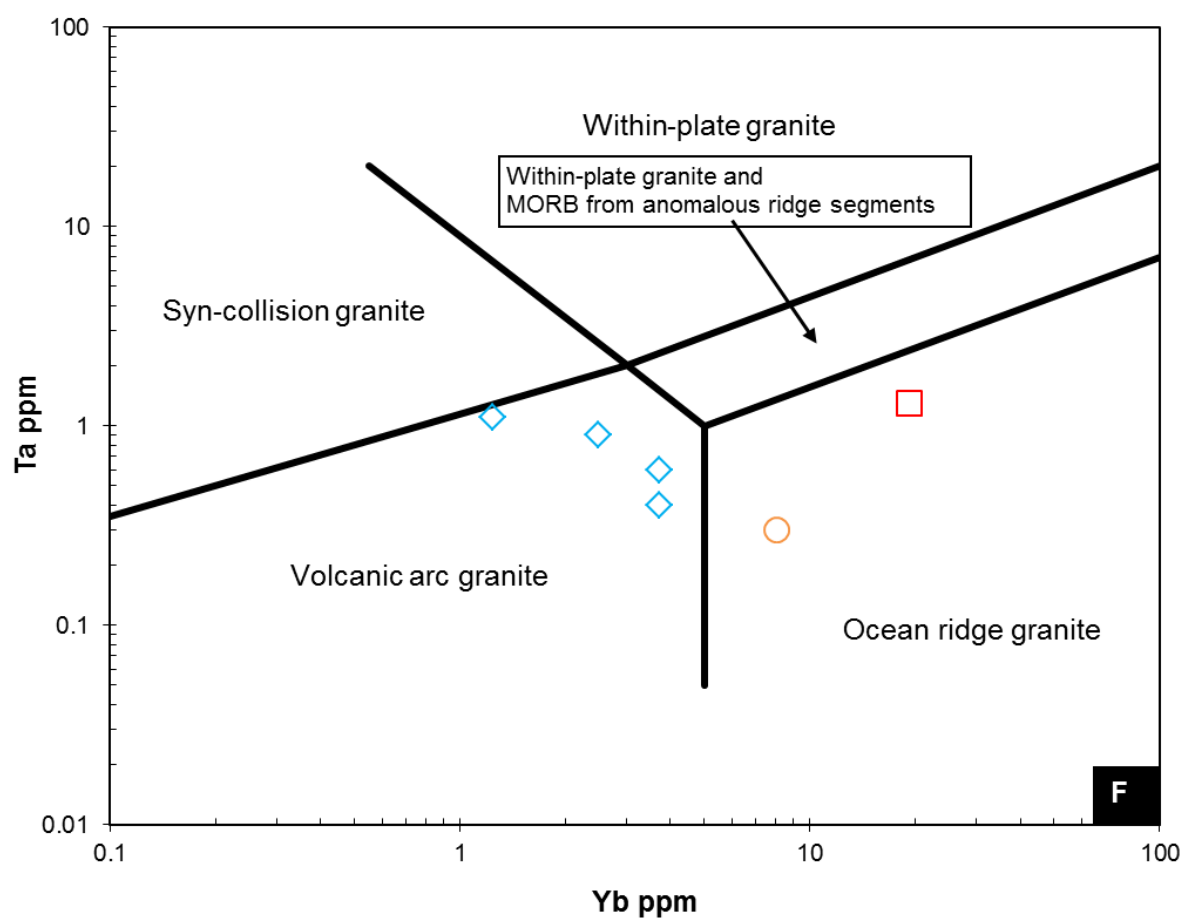
Figure 13F

Figure 14

Figure 15
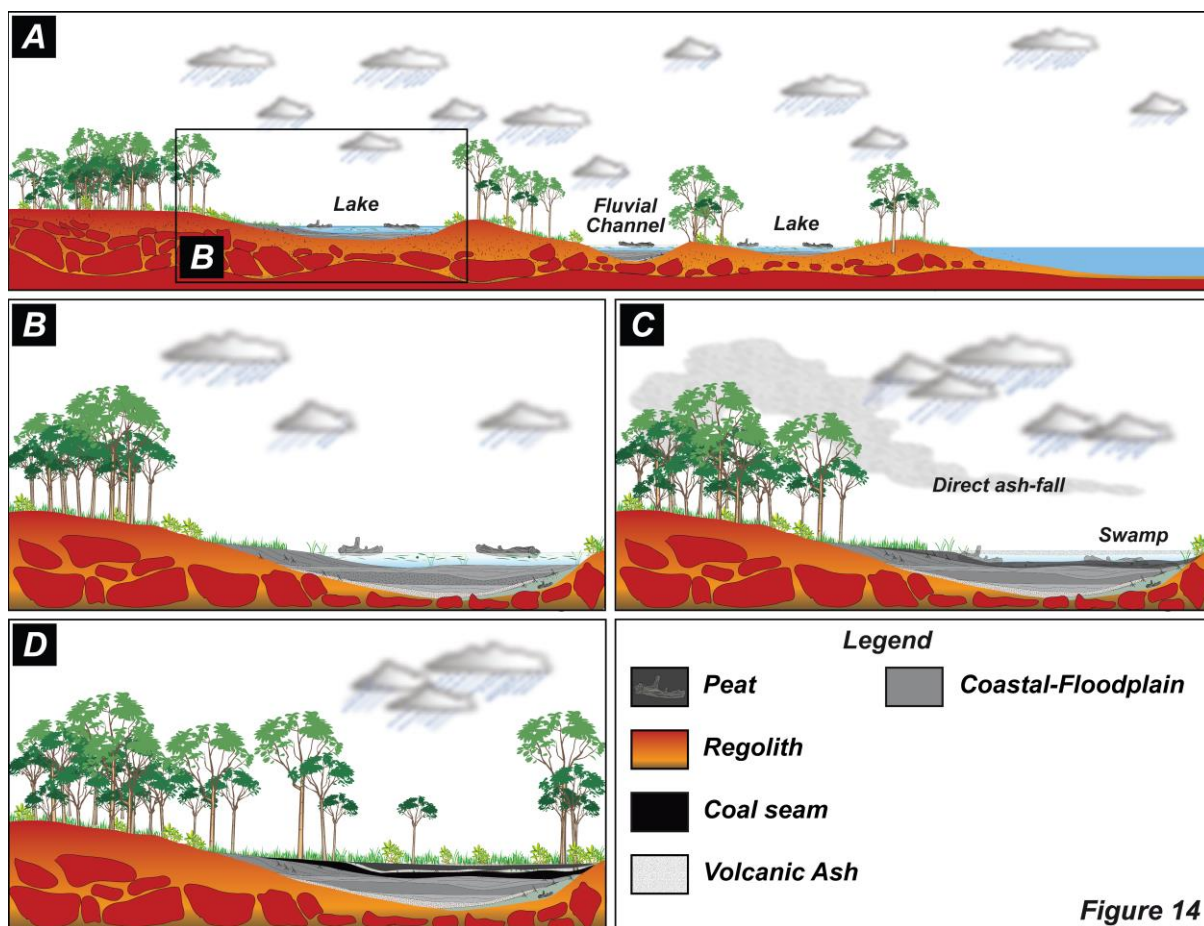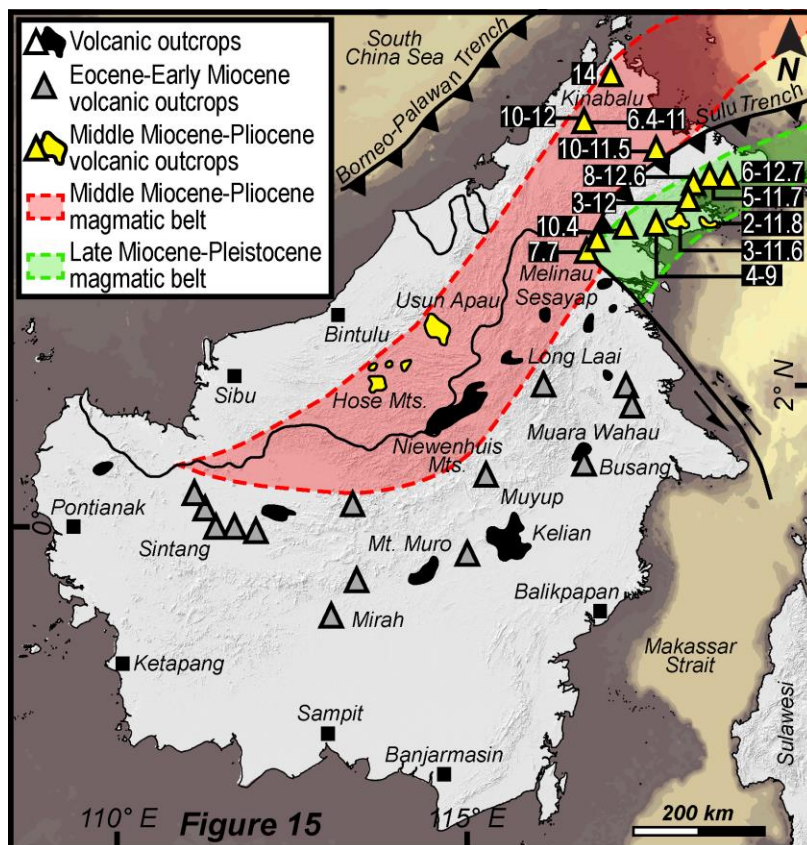
Graphical abstract
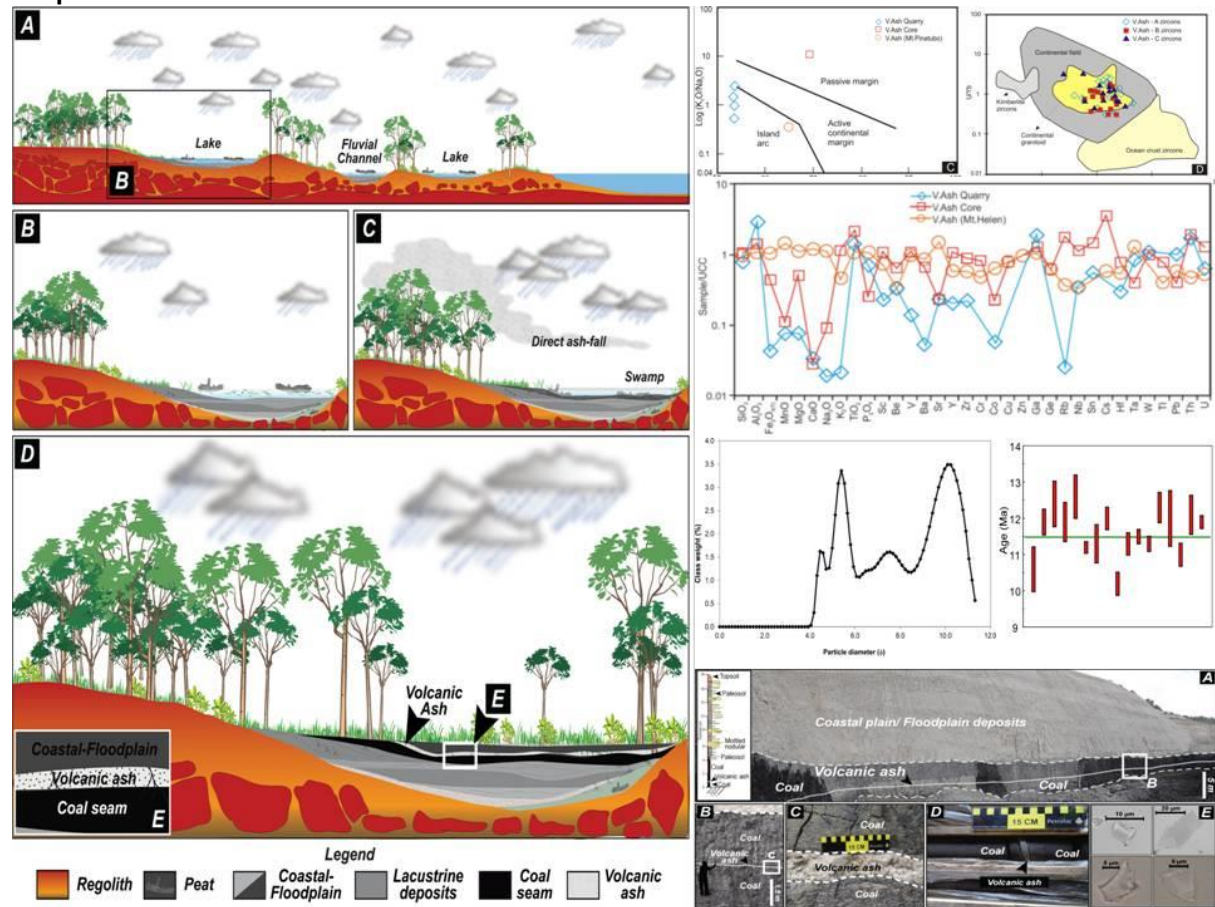
Table 1. Carbon content and loss on ignition of the studied ash and coal samples

SAMPLE NAME	Moisture (wt. %)	Organic C (wt. %)	Carbonate (wt. %)	Inorganic C (wt. %)	Total LOI (wt. %)
A (Ash)	3.2	8.5	15.5	11.4	23.1
B (Ash)	3.2	10.2	15.3	11.3	24.6
C (Ash)	4.0	14.0	13. 8	10.0	28.3
B TOP (Coal)	9.4	46.8	8.1	6.0	62.2
B BOTTOM (Coal)	10.0	52.4	8.8	6.5	69.0

Table 2. Major oxides (wt. %), trace and rare earth elements (ppm) data of the volcanic ashes from quarry, core and reference samples

Sample No.	A1	A2	B	C	VA 37	Reference Volcanic Ash
Origin (location)		Quarry section			Core	Mt. Pinatuba
Major oxides (in wt. %)						
SiO_2	43.0	40.0	41.4	41.7	62.4	63.5
SiO_2 adj	53.0	53.5	53.4	53.4	69.1	64.7
Al_2O_3	36.7	33.4	34.8	35.4	20.0	16.0
$Fe_2O_3(T)$	0.12	0.3	0.14	0.11	1.8	4.6
MnO	0.004	0.007	0.004	0.004	0.008	0.12
MgO	0.09	0.2	0.2	0.13	1.04	2.4
CaO	0.05	0.08	0.2	0.16	0.11	5.0
Na_2O	0.02	0.02	0.09	0.11	0.33	4.0
K_2O	0.03	0.05	0.09	0.06	3.6	1.5
TiO_2	0.62	0.66	0.58	0.39	0.9	0.55
P_2O_5	0.05	0.2	0.07	0.09	0.04	0.2
LOI	19.4	24.7	22.3	21.7	8.7	1.4
Tot	100	99.5	99.9	99.9	99	99.5
SiO_2/Al_2O_3	1.2	1.2	1.2	1.2	3.0	4.0
Al_2O_3/TiO_2	59	50.7	60.2	91.0	20.4	29
CIA	99.6	99.3	98.5	98.5	81	48
Trace and rare earth elements (in ppm)						
Sc	3	4	3	3	15	10
Be	< 1	1	< 1	< 1	2	1
V	18	22	15	7	119	105
Ba	15	48	35	24	379	466
Sr	10	209	55	52	84	519
Y	3	4	6	6	24	13
Zr	53	60	39	25	173	110
Cr	< 20	< 20	< 20	< 20	70	40
Co	< 1	1	< 1	< 1	4	11
Cu	< 10	< 10	< 10	< 10	20	20
Zn	< 30	< 30	< 30	< 30	< 30	70
Ga	34	31	31	38	22	18
Ge	< 1	< 1	< 1	< 1	1	1
Rb	< 2	< 2	3	< 2	201	42
Nb	7	6	3	2	14	4
Sn	4	4	2	2	3	< 1
Cs	< 0.5	< 0.5	< 0.5	< 0.5	17	3
Hf	2	3	1	1	5	3
Ta	1.1	1	0.6	0.4	1	0.3
W	2	3	2	2	2	< 1
Tl	< 0.1	< 0.1	< 0.1	< 0.1	0.6	0.3
Pb	6	33	15	< 5	7	10
Th	15	23	19	18	21	5
U	2	2	2	1	4	2
Th/U	8	10.3	8.4	16.5	6	3
Zr/Hf	27	22	28	25	38	36
Nb/Ta	6.4	6.7	5	5	11	13
Zr/Ti	0.01	0.01	0.01	0.01	0.03	0.03
Zr/Sc	17.7	15	13	8	11.5	11
Th/Sc	5.1	5.7	6.2	6	1.4	0.5
Ti/Th	301	233	242	165	309.9	670
La/Th	0.03	1.3	1.1	0.5	2.4	3
Ti/Zr	87	88	115	119	37.6	30
La	0.5	29	21	10	50	16
Ce	2.1	54	46	24	99	33
Pr	0.4	5.4	5.3	3	11	4
Nd	1.6	17	18	10	37	15
Sm	0.5	3	4	2	7	3
Eu	0.08	0.5	0.6	0.3	1.3	0.9
Gd	0.4	2	2	1	5	3
Tb	< 0.1	0.3	0.4	0.2	0.8	0.4
Dy	0.4	1.5	2	1.3	4.8	3
Ho	< 0.1	0.2	0.3	0.2	0.9	0.5
Er	0.2	0.5	0.7	0.7	2.9	1.4
Tm	< 0.05	0.1	0.1	0.1	0.5	0.21
Yb	0.2	0.4	0.6	0.6	3	1.3
Lu	< 0.01	0.1	0.1	0.1	0.5	0.22
∑REE	6.4	114	100	53	223	82
Computed ratios						
$(La/Yb)_{CN}$	1.7	48	23	11	11	8
Eu/Eu*	0.6	0.6	0.6	0.5	0.7	1

Table 3a. LA-ICP-MS trace element data (ppm) for the zircons retrieved from LFM-V.ASH-A (n=23)

Samp. No / Element	A (n=23)																						
	4	5	6	7	8	10	11	15	16	18	24	25	27	28	29	32	33	34	36	39	40	41	42
La	0.02	0.6	2.6	0.9	18	0.1	0.10	0.20	1.2	0.02	3.20	0.01	1.1	5	0.04	0.04	33	0.1	0.2	0.02	2	0.12	0.01
Ce	10	7	15	8	48	7	16	6	17	11	15	4	39	29	13	6	99	12	2	7	15	7	26
Pr	0.2	0.2	1.1	0.3	6	0.1	0.4	0.1	0.5	0.1	1.0	0.1	0.6	0.9	0.03	0.1	10	0.3	0.2	0.1	0.8	0.1	0.04
Nd	2.9	1.8	5.3	1.6	27	0.7	6.3	1.4	3.7	2.2	5.6	1.3	6.2	4.6	0.4	0.6	52	5	3	2.5	6	0.9	0.5
Sm	7	2.4	4	2.2	7	2.6	14.4	3.3	5	7	4	3.3	12.6	4	1.2	2.2	16	9	6	5	7.4	2.5	1.5
Eu	0.9	0.2	0.3	0.2	0.6	0.2	1.5	0.4	0.6	1.3	0.4	0.2	2.3	1.1	0.45	0.2	0.4	2	0.6	1	1.2	0.3	0.3
Gd	40	16	20	12	18	210	77	17	38	49	20	20	73	17	5	18	41	39	31	30	35	17	8
Tb	14	6	8	6	6	9	27	6.	155	20	8	8	28	6	2	8	13	13	11	11	12	7	3
Dy	169	82	113	63	73	129	316	78	207	236	99	103	361	75	28	105	162	156	130	145	146	95	43
Ho	63	34	47	27	29	55	112	32	84	86	41	40	143	31	11	46	62	5	48	57	55	40	17
Er	273	168	239	134	145	272	469	156	398	379	203	185	673	157	60	235	273	278	207	270	249	199	85
Tm	54	37	55	31	32	62	89	36	85	78	47	39	145	36	15	54	55	62	40	59	52	46	19
Yb	508	388	592	325	340	658	798	384	864	764	500	379	1470	392	179	578	506	647	377	612	511	493	205
Lu	89	75	114	64	66	127	133	76	158	142	100	68	274	79	38	112	83	143	65	113	93	97	38
Y	1856	1069	1510	834	916	1703	3238	1015	2542	2720	1304	1214	4468	1042	383	1490	1773	1896	1465	1765	1665	1283	534
ΣREE	1229	819	1217	673	814	1342	2058	793	1878	1776	1045	849	3229	837	354	1169	1405	1404	921	1312	1186	1004	447
(La/Sm)$_{CN}$	0.002	0.17	0.46	0.024	1.55	0.02	0.005	0.04	0.14	0.02	0.54	0.003	0.05	0.8	0.002	0.01	1.27	0.009	0.02	0.002	0.18	0.03	0.01
(Gd/Yb)$_{CN}$	0.06	0.03	0.03	0.03	0.04	0.03	0.08	0.04	0.04	0.05	0.04	0.04	0.04	0.03	0.02	0.03	0.07	0.05	0.07	0.04	0.06	0.03	0.03
Eu/Eu*	0.2	0.1	0.1	0.1	0.2	0.1	0.1	0.2	0.1	0.2	0.2	0.1	0.2	0.4	0.4	0.1	0.04	0.3	0.1	0.2	0.2	0.1	0.3
Pb*	0.5	2.1	3.8	1.2	1.4	3.5	1	1.3	3	1.7	2.1	80	58	17	15	3.6	37	2.3	0.6	1.3	1.2	2.5	43.3
Th^{232}	175	380	537	156	257	519	365	223	761	306	545	125	810	190	88	590	176	480	77	316	340	559	90
U^{238}	206	838	1174	349	470	1774	397	533	1256	803	919	359	926	184	174	1603	230	719	122	556	447	1109	170
Th/U	0.9	0.5	0.5	0.5	0.6	0.3	0.9	0.4	0.	0.4	0.6	0.3	0.9	1	0.5	0.4	0.8	0.7	0.6	0.6	0.8	0.5	0.5
U/Yb	0.4	2.2	2	1.1	1.4	2.7	0.5	1.4	1.5	1.1	1.8	1	0.6	0.5	1	2.8	0.5	1.1	0.3	0.9	0.9	2.3	0.8

ND-Not Determined

Table 3b. LA-ICP-MS trace element data (ppm) for the zircons retrieved from LFM-V.ASH-B (n=19)

Samp. No / Element	B (n=19)																		
	4	8	9	10	11	12	13	15	17	18	19	20	24	27	29	33	34	35	36
La	0.4	0.05	0.40	0.02	0.04	0.1	0.03	3.3	0.02	1.4	1	0.2	0.5	1.2	0.7	0.04	0.9	0.1	0.03
Ce	7	13	8	11	3	12	7	40	23	15	22	7	4	9	14	6	5	10	5
Pr	0.1	0.08	0.2	0.04	0.2	0.3	0.3	1.1	0.02	0.6	0.3	0.1	0.1	0.5	0.3	0.2	0.2	0.1	0.1
Nd	1.3	1.6	1.4	1	3	5.5	5	6	0.7	5.7	2	1.3	1.5	3.2	2.6	3.4	2	1.3	1
Sm	1.8	2.6	2.3	3.3	7.1	11	9.5	5	1.5	8	2.1	2.2	4	2.6	4.7	6.3	3.1	2.8	2.5
Eu	0.3	1.1	0.3	0.5	0.5	2	1.4	1.6	0.6	1.7	0.9	0.4	0.8	0.2	0.5	0.8	0.4	0.6	0.3
Gd	11	15	12	26	38	53	52	22	9	39	11	14	25	17	26	33	17	15	15
Tb	4.2	5.6	5	11	13.6	17.7	18.3	8	3.3	13.3	4.6	5.5	8.5	7.4	10	12	6	5.2	5.4
Dy	55	75	66	148	161	206	20	101	42	161	61	75	99	103	133	141	74	65	68
Ho	22	33	27	62	59	75	75	40	18	62	25	32	35	43	54	52	28	24	25
Er	113	178	136	296	255	329	317	190	91	288	125	160	155	215	261	226	126	112	111
Tm	25	44	31	64	50	66	61	43	22	62	29	37	33	50	60	45	26	24	23
Yb	268	516	322	648	467	631	556	442	260	625	320	396	333	529	622	421	245	232	215
Lu	53	113	62	121	79	113	93	82	55	115	65	78	64	101	119	72	44	42	37
Y	708	1113	852	1854	1717	2224	2195	1237	578	1899	822	1014	1107	1374	1695	1557	855	743	755
ΣREE	563	998	672	1391	1137	1521	1404	985	526	1397	670	808	762	1083	1307	1019	578	534	508
(La/Sm)$_{CN}$	0.12	0.01	0.11	0.004	0.003	0.005	0.002	0.41	0.01	0.12	0.29	0.05	0.09	0.29	0.09	0.004	0.19	0.02	0.01
(Gd/Yb)$_{CN}$	0.03	0.02	0.03	0.03	0.07	0.07	0.08	0.04	0.03	0.05	0.03	0.03	0.06	0.03	0.03	0.06	0.06	0.05	0.06
Eu/Eu*	0.2	0.5	0.2	0.2	0.1	0.3	0.2	0.5	0.5	0.3	0.5	0.2	0.2	0.1	0.1	0.2	0.2	0.3	0.2
Pb*	ND	9.9	1	2.3	0.6	1	0.5	6	18	6	5.3	1.2	ND	3.5	2.8	0.5	ND	14	0.3
Th^{232}	ND	151	201	606	124	299	156	272	88	404	154	221	ND	556	925	104	ND	131	54
U^{238}	ND	211	407	1002	200	357	172	388	200	488	284	464	ND	1529	1155	135	ND	293	81
Th/U	ND	0.7	0.5	0.6	0.6	0.8	0.9	0.7	0.4	0.8	0.5	0.5	ND	0.4	0.8	0.8	ND	0.5	0.7
U/Yb	ND	0.4	1.3	1.6	0.4	0.6	0.3	0.9	0.8	0.8	0.9	1.2	ND	2.9	1.9	0.3	ND	1.3	0.4

ND-Not Determined

Table 3c. LA-ICP-MS trace element data (ppm) for the zircons retrieved from LFM-V.ASH-C (n=17)

Samp. No	C (n=17)																
Element	1	2	3	4	5	6	8	9	10	13	14	15	16	18	19	21	22
La	0.02	8.2	0.6	0.1	0.02	0.2	0.03	0.1	7.1	0.2	0.3	11	0.4	0.2	0.5	0.6	0.1
Ce	2.5	25	33	4	8	16	6	19	28	6	9	47	11	8	11	15	7
Pr	0.3	2.3	0.5	0.2	0.05	0.2	0.07	0.09	3	0.1	0.2	4.5	0.3	0.1	0.2	0.7	0.05
Nd	5.3	11.5	5.2	1.2	0.9	2.5	1.4	1.4	14.2	1.4	1.8	27.5	3.1	2.2	1.9	5.6	0.5
Sm	12.3	9.3	6.8	3	2.5	3.6	3	2	6.4	3.2	3.8	15	6	4.8	2.9	6.7	0.7
Eu	0.4	1.5	2.7	0.8	0.4	1.1	0.5	0.7	0.4	0.3	0.6	1.7	0.9	0.5	0.4	2.3	0.3
Gd	65	40	30	15	16	15	19	10	24	19	23	59	36	30	17	29	4
Tb	24	14	11	5	6	5	7	4	9	7	9	20	14	12	7	11	2
Dy	291	171	121	52	74	50	99	43	123	98	126	234	177	157	87	137	19
Ho	108	67	42	17	29	19	41	17	52	41	52	85	72	65	35	51	7
Er	464	311	185	70	128	84	203	84	253	197	252	357	338	314	166	239	36
Tm	93	70	38	16	27	18	46	20	59	44	56	68	73	71	37	52	8
Yb	852	721	371	155	253	191	480	225	625	456	578	622	730	751	380	526	91
Lu	146	136	67	28	45	36	92	45	120	87	110	105	134	137	70	96	17
Y	3117	2043	1272	551	863	584	1268	549	1600	1241	1615	2370	2185	1963	1076	1626	238
ΣREE	2065	1588	914	366	588	441	998	471	1324	959	1222	1656	1594	1552	814	1172	191
$(La/Sm)_{CN}$	0.001	0.6	0.05	0.03	0.01	0.04	0.01	0.03	0.7	0.04	0.04	0.5	0.05	0.03	0.1	0.05	0.1
$(Gd/Yb)_{CN}$	0.06	0.05	0.07	0.08	0.05	0.06	0.03	0.04	0.03	0.03	0.03	0.08	0.04	0.03	0.04	0.04	0.03
Eu/Eu*	0.04	0.2	0.6	0.4	0.2	0.4	0.2	0.5	0.1	0.1	0.2	0.2	0.2	0.1	0.2	0.5	0.6
Pb*	28	2	21	49	1	73	ND	3	ND	2	2	8	2	2	2	228	85
Th^{232}	190	365	244	79	76	77	ND	98	ND	243	448	244	325	437	414	282	147
U^{238}	426	695	274	509	117	133	ND	172	ND	507	727	410	532	978	660	829	296
Th/U	0.5	0.5	0.9	0.2	0.7	0.6	ND	0.6	ND	0.5	0.6	0.6	0.6	0.5	0.6	0.3	0.5
U/Yb	0.5	1	0.7	3.3	0.5	0.7	ND	0.8	ND	1.1	1.3	0.7	0.7	1.3	1.7	1.6	3.3

ND-Not Determined